Dissertation

submitted to the

Combined Faculty of Natural Sciences and Mathematics

of the Ruperto Carola University Heidelberg, Germany

for the degree of

Doctor of Natural Sciences

Presented by

M.Sc. Lara Barteczko

born in: Gehrden, Germany

Oral examination: 14.12.2021

A study of oxytocin effects within the medial entorhinal cortex-hippocampus domain in rats

Referees: Prof. Dr. Rainer Spanagel

Prof. Dr. Valery Grinevich

Table of Contents

List of Abbreviations

µ	micro
2YT medium	yeast extract and tryptone medium
AAV	adeno associated virus
AN	accessory nuclei
BL	blue light
c	centi
CA	*cornu ammonis*
Ca^{2+}	calcium ions
$CaCl_2$	calcium chloride
Ch2R	channelrhodopsin 2
CNO	clozapine N-oxide
CO_2	carbon dioxide
COUP-TF	chicken ovalbumin upstream promoter transcription factor
Ctip2	COUP-TF interacting protein 2
dCA2	dorsal hippocampus CA2 region
DIO	double-floxed inverted open reading frame
DG	dentate gyrus
DMEM	Dulbecco's modified eagle medium
DNA	desoxyribonucleic acid
DREADD	Designer Receptors Exclusively Activated by Designer Drugs
EC	entorhinal cortex
EDTA	ethylenediamine tetraacetic acid
EF1a	elongation factor 1-alpha
EPSC	excitatory postsynaptic current
ETS	E twentysix
Etv1	ETS variant 1
FBS	fetal bovine serum
FLP	recombinase flippase
FRT	short flippase recognition target

FS	fast spiking
GABA	Gamma-aminobutyric acid
GAD67	Glutamate decarboxylase
GFP	green fluorescent protein
h	hour
HBS	Hepes buffered saline
HEK293T	human embryonic kidney 293T
i.p.	intra peritoneal
IPSC	inhibitory postsynaptic current
L	liter
LB	lysogeny broth
LEC	lateral entorhinal cortex
m	meter
magnOT	magnocellular oxytocin neurons
MEC	medial entorhinal cortex
min	minute
ml	milliliter
mm	millimeter
MS	medial septum
NaCl	sodium chloride
NaDoc	sodium desoxycholate
Na_2HPO_4	sodium phosphate
NeuN	Hexaribonucleotide binding protein 3
NGS	normal goat serum
OT	oxytocin
OTR	oxytocin receptor
OTR-IRES-Cre rats	oxytocin receptor knock-in Cre rats
parvOT	parvocellular oxytocin neurons
PBS	phosphate buffered saline
PC	pyramidal cell or principal cell

PCP4	Purkinje cell protein 4
PFA	paraformaldehyde
P/S	penicillin streptomycin
PV	parvalbumin
PVN	paraventricular nucleus
RFP	red fluorescent protein
rpm	revolutions per minute
RT	room temperature
sec	second
SLM	*stratum lacunosum-moleculare*
SOC medium	super optimal broth with catabolite repression medium
SON	supraoptic nucleus
SP	*stratum pyramidale*
vCA1	ventral hippocampus CA1 region

Summary

Spatial navigation and social behavior are two core processes throughout the life of animals and humans. The hippocampal subregions and the medial entorhinal cortex are known as the hub structures for spatial navigation and spatial memory. Locations and territorial borders encoded in spatial maps are often social in nature. However, it remains largely unknown how these social locations become encoded in the spatial maps.

Oxytocin (OT) is the evolutionarily conserved hypothalamic neuropeptide involved in emotional behaviors, such as anxiety and fear, as well as complex social behaviors. In mammals OT is produced exclusively in the hypothalamic nuclei, which project axons to the posterior pituitary, while axon collaterals target more than 50 forebrain regions, including the entorhinal cortex (EC). My PhD project aimed to explore the role of OT signaling within the MEC and to reveal its possible role in regulation of spatial and goal-directed navigation in a social context.

Employing cell-type specific recombinant adeno-associated viruses (AAVs), I identified profound axonal innervation of all layers of MEC by axons of OT neurons in adult female rats. Next, I investigated types of OTR-expressing neurons in the MEC utilizing newly generated female OT receptor (OTR)-IRES-Cre knockin-rats in combination with Cre-dependent AAVs. At anatomical level I found two distinct types of OTR+ neurons in the MEC: principal pyramidal cells (PCs) located predominantly in layer III and parvalbumin-positive interneurons scattered throughout the extend of the entire MEC.

To tackle the functional role of MEC OTR+ neurons, I initially used the AAV-based Designer Receptors Exclusively Activated by Designer Drugs (DREADD) system to specifically silence OTR+ neurons in the MEC of adult female OTR-IRES-Cre rats in social recognition and T-maze tests. I did not observe a significant difference between animals with silenced OTR+ MEC cells and controls in both behavioral tests. However, OTR+ cells were only silenced during the testing in the T-Maze, thus, not affecting the memory acquisition phase. To cover the entirety of the memory process, in the next set of experiments, I eliminated OTR+ MEC neurons by Cre-dependent AAV, expressing modified Caspase 3, injected to OTR-IRES-Cre female rats followed by the same behavioral tests. After confirmed elimination of virtually all OTR+ MEC neurons, no differences between groups were found in the social memory test. However, in the T-Maze test the group with ablated OTR+ MEC neurons was impaired in learning of the location of a conspecific but not of a food reward. This suggests that OTR+ MEC neurons might be involved in the generation of a memory engram for the spatial location of a conspecific and in the navigation towards this location, and that the OT-sensitive MEC→CA1 pathway can modulate spatial-social navigation in rats.

Zusammenfassung

Räumliche Navigation und soziales Verhalten sind zwei grundlegende Prozesse im Verlauf des Lebens von Tieren und Menschen. Die Hippocampus Subregionen und der mediale entorhinale Cortex (MEC) sind bekannt als die zentralen Strukturen für räumliche Navigation und Erinnerung. Die in räumlichen Karten kodierten Orte und territorialen Grenzen sind in ihrer Natur oft sozial geprägt. Allerdings bleibt es größtenteils unbekannt wie diese sozialen Orte in räumlichen Karten kodiert werden.

Oxytocin (OT) ist das evolutionär konservierte hypothalamische Neuropeptid, welches in emotionalen und komplexen sozialen Verhaltensweisen involviert ist. In Säugetieren wird OT ausschließlich in den hypothalamischen Nuklei produziert, von wo Axone zum Hypophysenhinterlappen verlaufen, während Axon Kollateralen mehr als 50 frontale Gehirnregionen innervieren, darunter den entorhinalen Cortex (EC). Mein PhD Projekt hatte das Ziel die Rolle von OT Signalwegen im MEC und seine potentielle Rolle in der Regulierung von räumlicher und zielgerichteter Navigation in einem sozialen Kontext zu untersuchen.

Unter Verwendung von Zelltyp-spezifischen rekombinanten Adeno-assoziierten Viren (AAV), konnte ich starke axonale Innervation von allen MEC Schichten durch OT Neurone in adulten weiblichen Ratten identifizieren. Als nächstes untersuchte ich die OT Rezeptor (OTR) exprimierenden Neurone im MEC unter Nutzung der neu generierten weiblichen OTR-IRES-Cre knock-in Ratten und Cre-abhängiger AAVs. Auf der anatomischen Ebene fand ich zwei deutlich unterschiedliche Typen von OTR+ Neuronen: pyramidale Zellen (PCs) größtenteils zu finden in Layer III und Parvalbumin-positive Interneurone, die über den MEC verteilt sind.

Um die funktionale Rolle von OTR+ MEC Neuronen zu untersuchen, habe ich zuerst das AAV-basierte Designer Receptors Exclusively Activated by Designer Drugs (DREADD) System verwendet, um spezifisch OTR+ MEC Neurone in adulten weiblichen OTR-IRES-Cre Ratten während eines sozialen Erinnerungstests und eines T-Maze Tests zu inhibieren. Ich konnte keine signifikanten Unterschiede zwischen den Tieren mit inhibierten OTR+ MEC Neuronen und der Kontrollgruppe beobachten. Allerdings wurden die Zellen nur während des T-Maze Tests inhibiert und die Modifikation hatte so keine Auswirkung auf die Erfassung der Erinnerung. Um den ganzen Erinnerungsprozess zu umfassen, wurde in den nächsten Experimenten ein Cre-abhängiger AAV, der modifizierte Caspase 3 exprimiert, in weibliche OTR-IRES-Cre Ratten injiziert. Nach der bestätigten Elimination annähernd aller OTR+ Neurone, wurden keine signifikanten Unterschiede im sozialen Erinnerungstest gefunden. Allerdings war die Gruppe mit eliminierten OTR+ MEC Neuronen im Lernen des Ortes einer sozialen Belohnung beeinträchtigt, aber nicht beim Lernen des Ortes einer Nahrungsbelohnung. Dies suggeriert, dass OTR+ MEC Neurone in der Bildung von Erinnerungsengramms der Orte von Artgenossen und der Navigation zu diesen Orten involviert sein könnten und dass der OT-sensitive MEC→Hippocampus Pfad räumliche-soziale Navigation in Ratten modulieren kann.

1. Introduction

Orienting in space is a core process needed to accomplish everyday life across species [1]. The medial entorhinal cortex (MEC)-hippocampus network is known as the hub structure for spatial navigation, harboring grid cells, place cells and other spatially tuned neurons [2,3,4]. Complex neuronal networks allow for formations of spatial memories, mapping of changing environments and navigation towards goal locations [5]. However, these internal spatial maps are not realized as such but as locations with a specific relevance. This relevance may be related to survival aspects such as a food location. Though, as mammals are overall social in nature a lot of locations can be defined by social aspects, such as a territory or a "home" location describing the place where familial conspecifics or a mated partner are residing [6,7].

Social behaviors are important throughout the life of all living creatures. In mammals, from childhood interactions with the mother, over play behaviors during adolescence to pair bonding, sexual behaviors and aggression in adulthood, the pro-social hypothalamic neuropeptide oxytocin (OT) plays a role in all these behaviors [8,9]. As basically all of these behaviors are tightly linked to specific locations or territorial borders, it would be logical to assume a link between OT and socially relevant spatial maps [10].

1.1 Medial entorhinal cortex (MEC)

The entorhinal cortex (EC) is part of the hippocampus region and tightly linked to the hippocampus by giving input signals and receiving output. Both structures play a critical role in memory formation and retrieval as well as in the construction of spatial maps of the environment [5,11]. The EC can be divided into the lateral (LEC) and medial (MEC) entorhinal cortices. The MEC and LEC provide the hippocampus with spatial and non-spatial information, respectively [12]. The MEC has mainly become known for harboring grid cells that give input to place cells in the hippocampus. However, further spatially tuned cell types have been discovered and the following sections will focus on MEC anatomy and function [5].

1.1.1 Anatomy

The MEC is located in the posterior part of the brain and elongated along the dorso-ventral axis (Figure 1A). It is a classical cortex composed of 6 layers [13]. Extrinsic inputs are mainly received in the superficial layers from regions such as for example different olfactory structures, the pre- and parasubiculum. However, inputs from infralimbic and prelimbic cortex innervate Layer V. Principal cells are located in layer II, III and V [14]. Figure 1B provides an

overview of relevant cell types and anatomical organization of the MEC, which will be explained in detail below.

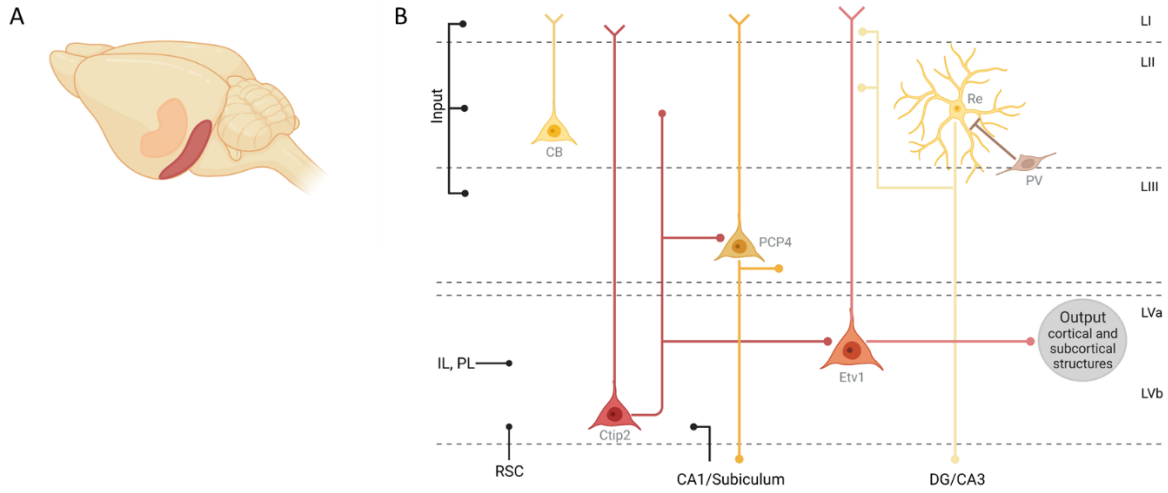

Figure 1: Anatomy of the MEC. (A) Location of the MEC (red) in the rat brain. Created with BioRender.com (B) Schematic drawing of the MEC intracellular network, based on Witter et al., 2017 [14]. Created with BioRender.com

Layer II is composed mainly of medium-sized excitatory pyramid cells (PCs) and large multipolar neurons known as Stellate cells. Layer II PCs can be identified by calbindin staining, while stellate cells specifically express reelin. In mice calbindin pyramid cells are clustered in patches, but in most parts of the MEC in other species this clustering is not found. Their projections go to different regions including CA1 region of the hippocampus, contralateral EC and the olfactory bulb. In contrast, stellate cells project to the dentate gyrus (DG) and CA3 region of hippocampus [14]. Aside from principal cells, MEC contains different groups of interneurons, the largest subgroup being parvalbumin (PV) positive interneurons. PV-positive interneurons have a fast-spiking electrophysiological phenotype [14,15]. PV-positive basket cells surround principal cells in layer II and can inhibit both types of principal cells [16], though they mainly seem to form synaptic connections on Stellate cells. The second PV-positive interneuron type are Chandelier cells (also known as axo-axonic cells) characterized by their axonal boutons making synapses on the initial axonal segments of principal cells. These interneurons are located in both layer II and III. Other interneuron types are somatostatin and $5HT_{3A}$ interneurons [14]. Through electrophysiological pair recordings it has been shown that the interneurons in MEC layer II are crucial for the functionality of the intrinsic network. For example, Stellate cells do not form connections with other Stellate cells and are solely connected through intermediate interneurons [14,15].

Compared to layer II, much less is known about layer III neurons. The principal cells in layer III are for the most part spiny excitatory pyramid neurons that project to CA1 region of the hippocampus and to subiculum. They also send axon collaterals to the contralateral EC region

and hippocampus [17]. They can be marked by Purkinje cell protein 4 (PCP4), which stains principal neurons in layer III and layer V of the MEC [18]. There is a variety of different interneurons in layer III. The intrinsic connections have not been as deeply investigated. However, in contrast to layer II, principal cells in layer III form monosynaptic connections with each other [14].

Layer V of the MEC is comprised of two sublayers, layer Va and layer Vb. The more superficial layer Va is the main output layer of the entorhinal cortex, providing input to many different cortical and subcortical regions. Cells in layer Va are big pyramidal neurons expressing E twentysix (ETS) variant 1 (Etv1). In contrast, layer Vb neurons are smaller and express chicken ovalbumin upstream promoter transcription factor (COUP-TF) interacting protein 2 (Ctip2). Layer Vb neurons receive input from the hippocampus and superficial layers of the MEC [14,19]. Interestingly, they also give rise to intrinsic projections to layer Va neurons and neurons in layer II and III, thus providing a major component of the deep to superficial circuit in MEC. This is also relevant for the hippocampus-memory system, as they mediate hippocampus output through their connection to layer Va neurons and form a feedback loop by projecting back to layer II and III neurons [20].

1.1.2 Spatially tuned cells

The first cells to be discovered that fired in a spatially tuned manner were place cells in the hippocampus. Place cells fire specifically when the animal is at a certain location, thus inciting their name.

In the MEC there are different types of spatially tuned cells (Figure 2). In the dorsal MEC grid cells, head direction cells, border cells, speed cells and recently object-vector cells have been discovered [2,5,11,21]. As their name suggests, head direction cells fire in a certain orientation of the animal's head [22], while border cells mark the borders of an environment with their firing pattern [23] (Figure 2A). Speed cells fire in response to the running speed of the animal with their firing rates increasing linearly with the speed [24,25]. As the firing patterns of grid cells and object vector cells are more complex, they are described in detail below.

In bigger environments, grid cells fire in multiple locations with their firing fields forming periodic hexagonal patterns. Those patterns can vary in scale, orientation, and phase [2,26]. They can be found in all layers of the MEC but are mainly located in layer II [27]. Along the dorso-ventral axis of the MEC, the scale, which means the distance between the firing fields, increases from dorsal to ventral. As shown in Figure 2B grid patterns in the dorsal MEC have a small scale with many firing fields in an environment, while in the ventral MEC only a few firing fields are present in an environment of the same size [28]. Grid cells can be clustered into a

small number of modules that show the same grid scale [2,29]. They are essential for path integration and their input to hippocampus for the formation of place fields [5].

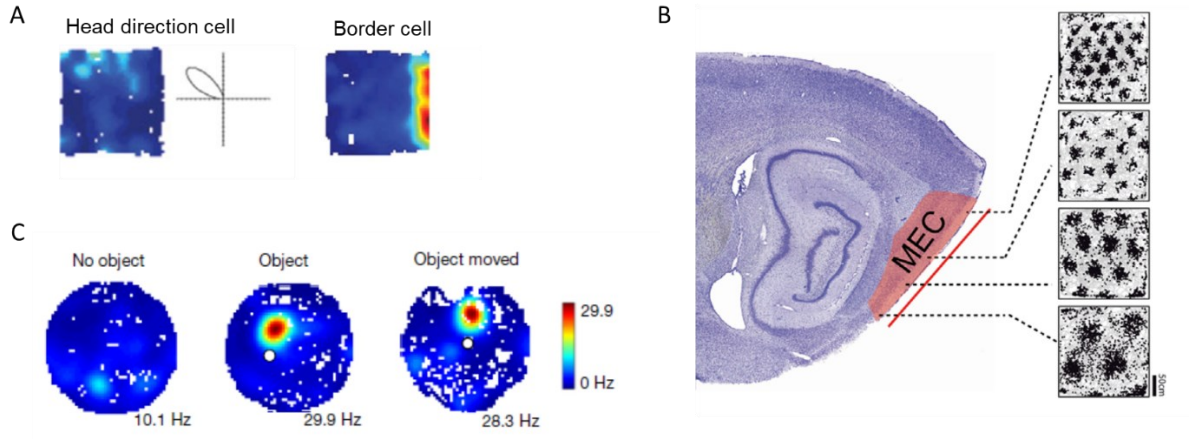

Figure 2: Spatially tuned cells in MEC. (A) Firing pattern of head direction and border cells. Reprinted from [5] with permission from Elsevier. (B) Grid cell firing patterns along the dorso-ventral axis of MEC. Reprinted from [5] with permission from Elsevier. (C) Firing pattern of object-vector cells upon inserting and moving an object in the environment. Reprinted by permission from Springer Nature Customer Service Centre GmbH: Springer Nature. NATURE. Høydal, Ø.A., Skytøen, E.R., Andersson, S.O. et al. Object-vector coding in the medial entorhinal cortex. Nature 568, 400–404 (2019). https://doi.org/10.1038/s41586-019-1077-7. Copyright 2019

Object-vector cells can be recorded in environments that contain discrete objects. It is known that animals use information about the location of objects for navigation. This information about the location of an object relative to the animal's own location is coded by object-vector cells. Object-vector cells are defined as cells that fire when the animal is positioned at a specific distance and direction from an object in the spatial environment. As shown in Figure 2C, the firing field of an object-vector cell moves in conjunction with the object when it is moved to a new location within the environment. Neurons that fire in a vector-like manner in relation to an object are found in superficial layers of the MEC and more abundant than other spatially tuned cells. Their firing fields are independent of the identity, size or location of the object and also not dependent on the head direction of the animal [21].

Taken together, all spatially tuned cells provide spatial information either to each other through intrinsic networks, and/or to the hippocampus for the formation of place fields. Unfortunately, most studies on spatially tuned cells in the MEC can only approximately define their location, thus making it difficult to relate spatial types of MEC cells to anatomically defined cell types.

1.1.3 MEC-Hippocampus network

The EC is the main structure providing input to and receiving output from the hippocampus. As described earlier, neurons from layer II of the MEC are projecting to the DG and CA3 of the hippocampus, while layer III neurons are projection to CA1 region. In the hippocampus, Schaeffer collaterals connect CA3 neurons to CA1 neurons (see Figure 3C) [30].

The hippocampus itself is composed of a ventral part preferentially involved in emotional and affective processes, and a dorsal part critical for memory and spatial functions. The dorsal hippocampus can be divided into 4 subdivisions: the DG in the center of the hippocampus structure and the *cornu ammonis* (CA) fields CA1, CA2 and CA3 on the outside (Figure 3A and B). These subdivisions are morphologically distinct with CA1 containing small pyramidal neurons and CA3 and CA2 having large pyramidal neurons with or without mossy fibers [31, 32]. The hippocampus has three layers (Figure 3B), a superficial molecular layer (*stratum orients*) on the outside, a cellular layer, also known as *stratum pyramidale* (SP), and a polymorph layer (*stratum radiatum,* SR). Only very few inhibitory neurons reside in the molecular layer. The cellular layer is packed with pyramid cells as well as some basket interneurons. The polymorph layer contains interneurons as well as excitatory neurons [30, 32]. One prominent type of interneurons are PV-positive basket cells in the cellular layer. They form inhibitory synapses on pyramidal cells (PC), preferentially targeting deep PCs [33]. This is one of presumably various microcircuits contributing to the complex structure of hippocampus network activity.

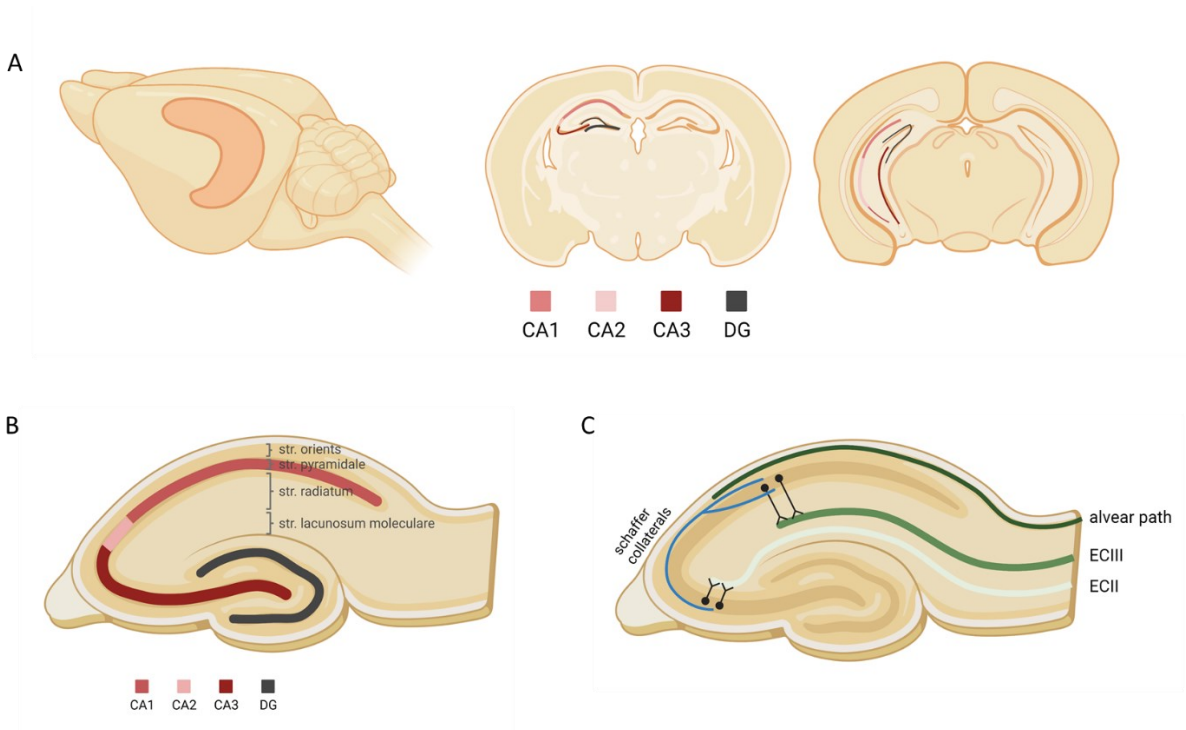

Figure 3: Hippocampus anatomy. (A) Overview of the hippocampus position in the rat brain and its subfields. Created with BioRender.com (B) Subfields and layers of the dorsal hippocampus. Subfields are

marked with different colors, as indicated in the legend below. Created with BioRender.com (C) EC input connections to hippocampus and intrahippocampal connections. Created with BioRender.com

In Figure 3C input connections from the MEC to the hippocampus are shown. As previously discussed, MEC layer II stellate neurons innervate the DG and CA3 region of hippocampus. The main pathway described for MEC layer II connections to hippocampus is the tri-synaptic pathway. MEC layer II stellates form synapses on DG, DG is projecting to CA3 pyramid neurons and CA3 pyramid neurons form synaptic connections on CA1 PCs known as Schaffer collaterals [30,32,34]. From MEC layer III PCs, two separate pathways innervate hippocampus. One, also known as temporo-ammonic pathway, enters through the *stratum lacunosum-moleculare* (SLM) above the DG and synapses on dendrites of PCs and interneurons. The other pathway, called alvear path, traverses through the stratum orients before also ending in the SLM. Axons of MEC Layer III neurons of the alvear path form synapses in the SLM but also synapse on CA1 PC and interneuronal dendrites in stratum orients [35]. For synapses in the SLM mostly feedforward inhibition of CA1 PCs has been described, meaning that excitatory glutamatergic synapses of MEC neurons evoke activation of interneurons that then inhibit CA1 PCs via Gamma-aminobutyric acid (GABA) signaling [35,36]. For the alvear pathway this has also been shown, still additionally monosynaptic input to PCs can be found that evokes subthreshold excitatory postsynaptic currents (EPSCs) though no action potentials. Both pathways seem to promote mainly feedforward inhibition, however, they can target different hippocampus interneuronal networks thus contributing in specific ways to the hippocampus network activity and different behavioral mechanisms [35]. Additionally, layer III MEC axons target deep PCs in proximal CA1 [37] which contributes to a distinction between MEC layer II and layer III input with the MEC layer II→DG→CA3→CA1 circuit primarily targeting superficial CA1 PCs while MEC layer III innervation preferentially engages deep PCs [34]. Interestingly, it has also been reported that both EC layer II and III innervate CA2 region of hippocampus [38], which is related to regulation of social memory [39,40]. This excitatory input leads to activation of CA2 neurons that have further excitatory connections to CA1 neurons [38].

Output from hippocampus to MEC can go directly from CA1 PCs to neurons in MEC layer Vb or indirectly from CA1 over dorsal subiculum to MEC layer Vb [30,41]. Neurons in layer Vb then relay the information to layer Va cells, which provide input to various cortical and subcortical regions [14,20].

1.2 Oxytocin (OT) system

1.2.1 Anatomy

Oxytocin (OT) is the evolutionarily conserved hypothalamic neuropeptide involved in social and emotional behaviors [42,43,44]. OT is exclusively produced in the hypothalamic nuclei and released into the bloodstream via the pituitary. Furthermore, OT neurons send axon collaterals into various brain regions acting on OT receptors (OTRs) and influencing local neuronal networks [45]. OT neurons reside in the paraventricular nucleus (PVN), supraoptic nucleus (SON) and accessory nuclei (AN) of the hypothalamus (Figure 4A). In the rat, the hypothalamus contains about 8000 OT neurons [46,47]. Traditionally, they are divided into two distinct types – large magnocellular (magnOT) neurons and smaller parvocellular (parvOT) neurons. Beside their morphology, these neurons also differ in their projections, electrophysiological characteristics, and functions. Most of OT neurons are magnOT neurons [46]. They provide the OT projections to the pituitary, thus, releasing OT into the bloodstream. Additionally, they send axon collaterals to various forebrain regions [46,48]. In contrast, parvOT neurons, found only in the PVN, are smaller and have an elongated, spindle-like morphology. They give rise to long axonal projections to hindbrain structures and send collaterals to SON magnOT neurons [49]. They only account for about 1% of all OT neurons but can strongly influence OT function by acting on magnOT neurons [46].

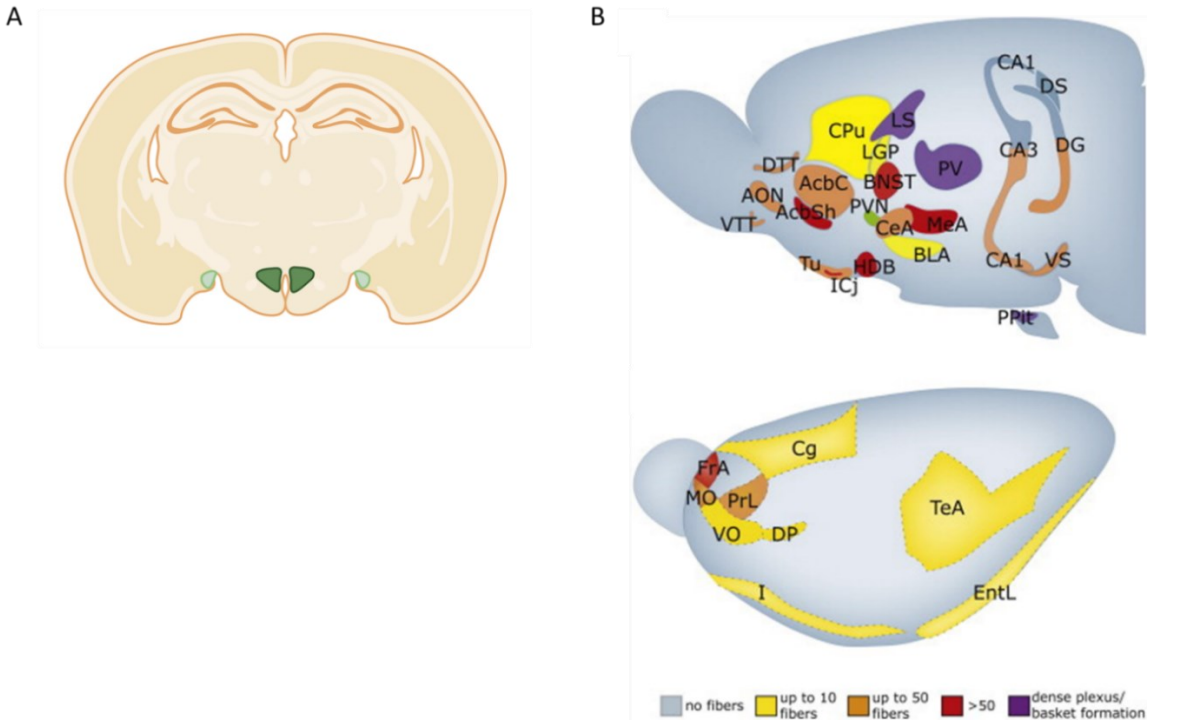

Figure 4: OT neurons and their axonal projections to the posterior pituitary and forebrain. (A) Location of PVN, marked in dark green on both sides of the third ventricle, and SON, indicated in light green lateral

next to the optic tract, in a coronal rat brain slice. Created with BioRender.com (B) Brain regions that receive axonal innervation from PVN OT neurons. Reprinted from [45] with permission from Elsevier.

Projections from magnOT neurons have been found in more than 50 forebrain and various hindbrain regions (Figure 4B). Adeno associated virus (AAV)-based tracing utilizing mouse OT promoter-driven expression of fluorescence proteins was employed to specifically label OT neurons and their distant axons. In respect to the EC-hippocampal domain, labeled OT axons have been shown in the lateral EC and ventral hippocampus, but not in the dorsal hippocampus [42,45]. Notably, OT innervation of the MEC was not investigated so far [45].

1.2.2 OT release and OT Receptors (OTR)

Extrahypothalamic OT axons usually have multiple terminal sites with varicosities, but rarely form synapses on neurons in the target forebrain regions. In response to afferent stimuli, action potentials occur in OT cells triggering Calcium ion (Ca^{2+}) influx at the axon terminals and exocytosis of dense core vesicles. Release of OT in target brain regions is likely to be synapse-independent resulting in diffused release of a dense core vesicle reaching target cells [50]. Furthermore, in the hypothalamus OT can be released from dendrites, which leads to synchronization of magnOT neuron activity and burst firing specifically during lactation [50,51].

OTRs are present in many different brain regions, largely overlapping with regions with reported OT innervation [52,53]. However, for some regions with reported OTR expression, such as the dorsal hippocampus, little or no OT innervation has been shown [42].

OTRs are G-protein coupled receptors, encoded by a single gene and highly conserved through evolution. OTRs are located at the cell membrane when no OT is present. Upon being exposed to OT, OTRs can be internalized to prevent hypersensitization of the cell and later recycled back to the membrane for reactivation [54]. Upon activation, OTRs can interact with different G proteins leading to activating or inhibiting intracellular cascades [53]. Which G proteins are recruited depends on the concentration of OT, with OT concentrations around the receptor's affinity leading to activating Gq protein cascades. Much higher OT concentrations are necessary to induce inhibitory signaling cascades. It is expected that OT concentrations around 1nM induce OTR coupling resulting in Gq activation, while concentrations of 10nM would be necessary to induce Gi/Go protein cascades. Density of OTR expression in different cells types can also contribute to the OT concentrations necessary for cellular activation. In general, it can be estimated that from the site of release one dense core vesicle may result in OT concentrations about 1nM in a spherical tissue volume of 55 μm and activate Gq in 2-3 OTR expressing cells [42,54,55].

1.2.3 OT function

OT modulates diverse emotional behaviors, such as anxiety and fear [56], as well as complex social behaviors [8,57,58]. In this section I will provide a short overview of OT's social functions in distinct brain regions.

As introduced earlier, OT is important in social interactions and socially relevant behaviors [8, 59]. OTRs are strongly expressed in regions that receive sensory input like the olfactory system in rodents and the visual system in monkeys. In the auditory system modulation by OT has also been described [47,60]. Recently, it has been shown that somatosensory stimuli, such as social touch, activate parvOT neurons in the PVN. ParvOT neurons transmit this excitation to magnOT neurons, leading to strong activation of OT neurons during social interactions in female rats [61]. This activation of OT neurons during social interactions increases the salience of the social sensory input, thus, leading to OT's pro-social effects in different social behaviors [8].

OT is generally involved in parental behaviors [62,63]. Intraventricular OT injection and evoked endogenous release of OT have been shown to trigger maternal behaviors in virgin female rodents [8,64], while interaction with mothers and observation of maternal behavior led to activation of OT neurons in virgin female mice [65]. In addition to parental behaviors, in monogamous prairie voles OT regulates pair bonding [66], meaning that the formation of partner preference is dependent on OT signaling in the nucleus accumbens during mating [8,67]. OT signaling is also relevant for other aspects of sexual behaviors such as the discrimination between male and female odors mediated by OT input to the medial amygdala [8]. Social communication and play behaviors are also influenced by OT [47,68]. Different recent experiments showed that appropriate responses in social contexts rely on OT action. For example, OT input to the amygdala is necessary for discrimination of positive and negative emotional states in mice [69]. Besides, social recognition, the ability to distinguish between familiar and novel conspecifics, was found to be enhanced by central injection of OT and conversely impaired in OTR knock-out mice [66]. As the hippocampus domain is involved in social memory, the role of the hippocampus and OT in social recognition will be discussed in detail in the next section.

1.3 Hippocampus and social behaviors

The hippocampus complex is mainly known for its role in spatial navigation and episodic memories [1]. However, hippocampal subregions are also involved in socially relevant

behaviors [70]. The next paragraphs will summarize the role of the hippocampus in socially linked behaviors and also studies concerning OT and OTRs in hippocampus.

As described in previous sections, OT neurons innervate mainly the ventral part of the hippocampus and have been scarcely found in the dorsal hippocampus [42,45]. OTRs are expressed in different hippocampus regions including DG, CA1, CA2 and CA3, though highest expression was detected in CA2 and CA3 [71,72]. In DG and CA1 the majority of OTR expressing cells are inhibitory neurons [73,74]. In contrast, in CA2 and CA3 regions mainly excitatory cells express OTRs [75,76]. It has been shown, that OTR activation enhances excitatory input in CA2/3 region and can alter the excitability and evoke firing of pyramid neurons [71,76,77]. OTR activation in interneurons also has an effect on their excitability and increases their inhibitory input on post-synaptic cells in CA1 region [78,74]. In general, it is proposed that OT action in the hippocampus influences the excitation/inhibition balance in hippocampus regions to increase the signal-to-noise ratio [71,74,78]. Similarly with the hippocampus, neurons of EC also express OTR mRNA [79], but cell types and their functional role remain to be further investigated.

Social information is one of several components of episodic memories. For animals living in social groups the ability to distinguish between different conspecifics is crucial to elicit appropriate behavior [59,70]. In multiple studies the CA2 region of the dorsal hippocampus (dCA2) was shown to be necessary for encoding of social memories [80,81,82]. Lesions of dCA2 as well as genetic inactivation of dCA2 pyramidal cells in transgenic mice resulted in impaired social memory [81,83]. Additionally, the ventral CA3 region is also necessary for encoding of social memories [71] while the EC→DG circuit is needed for recall of social memory [84].

It was shown that OTRs in DG and CA2/3 region of the hippocampus are important for discrimination between social but not non-social stimuli [73]. Besides, different OTR knock-out mice, including specific knock-out in CA2/CA3 region, show deficits in social memory [73,85]. Information is transferred from dCA2 to ventral CA1 region [71]. Thus, it fits that storage of social memory takes place in the CA1 region of the ventral hippocampus (vCA1). Pyramidal neurons in vCA1 encode social memory engrams and activation of such neuronal ensembles is sufficient to restore social memory [83,86]. EC connections to DG are also implied in the retrieval of social memories, with specific synaptic inhibition leading to impairments in social memory [84]. In summary, distinct hippocampal regions are necessary for social memory processing presumably with involvement of OTR expressing cells.

Spatial navigation and spatial memory are necessary to enable social interaction between conspecifics and find locations of social interest [7,87]. MEC input to hippocampus is necessary for normal acquisition of place memory, as was shown in MEC lesion studies where lesioned rats were impaired in water maze task, but not in other hippocampus-dependent tasks [88]. Recently, two studies highlighted MEC importance in goal-directed navigation and learning of

reward locations. Recording of cells in MEC showed that in a food reward learning task, firing location of cells shifted towards the reward location or firing frequency was increased closest to the reward location [89]. Firing fields of grid cells also moved towards the goal location. Furthermore, the number of cells in MEC and place cells in CA1 with the strongest firing field at the reward location increased during learning [90]. Importantly, it has also been recently reported that a subset of CA1 place cells displayed activation at the location of a conspecific animal specifically or additional to firing at the animal's own location [91]. It remains unknown how these place fields are generated in the entorhinal cortex-hippocampus network, though it is suggested, that distinct temporal combinations of inputs from both EC layer III and CA3 are relevant for generating specific CA1 activity in response to spatial stimuli. However, their existence supports the importance of the hippocampus in conjunction with the EC for social interactions [92]. Interestingly, a similar cell type, presumably involved in the encoding of social memory, was described in CA2 [93].

1.4 Aim of the thesis

Spatial navigation and social behaviors are core processes underlying navigation towards the location of social partners, life in social communities, formation of social hierarchy, or defense of the borders of their own territory [7,10,87]. However, it remains elusive what kind of anatomical and functional neuronal network links these processes. Based on the recent reports that OT modulates social memory encoding in the hippocampus [71,83], it is tempting to propose that this neuropeptide is involved in modulation of space navigation. However, in the dorsal hippocampus, which is controlling spatial encoding and memory, OT innervation is almost negligible [42]. On the other hand, the EC, a structure tightly connected with the dorsal hippocampus, is innervated by OT neurons [45] and expresses OTRs [79] and, hence, may transmit OT signaling towards the dorsal hippocampus.

Thus, the aim of this study was the exploration of fine anatomical connections of the OT system with the MEC-hippocampus junction as well as revealing the functional role of OT signaling within the MEC in social memory and spatial navigation of adult female rats.

2. Materials and Methods

2.1 Materials

2.1.1 Cell Culture

PBS	(Dulbecco´s) Phosphate buffered saline 1x (without calcium, magnesium)	Sigma Aldrich	#D8537-500ML
DMEM	Gibco Dulbecco´s modified eagle medium (DMEM) ((+)4.5 g/l glucose, (+)L-glutamine, (+)pyruvate, 1x, 500 ml, with phenol red)	Thermo Fischer Scientific	#41966052
FBS	Fetal bovine serum superior	Sigma Aldrich	#S0615-500ml
P/S	Gibco Penicillin Streptomycin (10000 U/ml)	Thermo Fischer Scientific	#15140122
Trypsin-EDTA	Gibco Trypsin-EDTA (0.05 %), with phenol red	Thermo Fischer Scientific	#25300054

2.1.1.1 Cell culture instruments

Cell culture hood Cellguard	Nuaire
CO_2 incubator Autoflow	Nuaire
Waterbath 1083	GFL
Centrifuge CL-G6S	Beckmann
Pipetboy 2	Integra

2.1.2 DNA preparation

LB-medium (Nutrient Broth,No. 1, for microbiology)	Sigma-Aldrich	#70122
Agar	Sigma-Aldrich	#A1296
2YT-medium	Sigma-Aldrich	#Y2377
Ampicillin	Thermo Fischer Scientific	#11593027
SOC-medium	Thermo Fischer Scientific	#15544034
HiSpeed Plasmid Maxi Kit (25)	Qiagen	#12663

2.1.3 AAV production and purification

Sterile water	Sigma-Aldrich	#W3500-500ML
$CaCl_2$	Sigma-Aldrich	#C5670
Sodium Phosphate Na_2HPO_4	Sigma-Aldrich	#S7907-100G
Hepes	Sigma-Aldrich	#H4034-100G
PBS tablets	Thermo Fischer Scientific	#18912014
Benzonase	Merck	#1.01654.0001
NaDoc (Sodium desoxycholate)	Sigma-Aldrich	#30970-25G
Tris Ultrapure	Applichem	#A1086,1000
Sodium Chloride NaCl	Sigma-Aldrich	#S7653-1KG
Hydrochloric acid HCl 37%	Sigma-Aldrich	#258148-500ML
HiTrap Heparin Columns 1\,ml	Cytiva	#17040601
Ambion Ultra-4 Centrifugal Filter Unit	EMD Millipore	#UFC810024
Acrodisc column Syringe filter (0,2 um Supor Membrane)	Pall Laboratory	#514-4122
10% Mini-PROTEAN Protein gel	Bio-Rad	#4561035
QC Colloidal Coomassie stain	Bio-Rad	#161-0803
2-Mercaptoethanol	Sigma-Aldrich	#M3148-25ML

2.1.3.1 Prepared buffers

2x HBS, pH 7.1	280 mM NaCl
	1.5 mM Na2HPO4
	50 mM HEPES
Collection buffer 150mM	150 mM NaCl
	20 mM Tris
Washing buffer 100mM	100 mM NaCl
	20 mM Tris
Washing buffer 200mM	200 mM NaCl
	20 mM Tris
Washing buffer 300mM	300 mM NaCl
	20 mM Tris
Elution buffer 400mM	400 mM NaCl
	20 mM Tris
Elution buffer 450mM	450 mM NaCl
	20 mM Tris
Elution buffer 500mM	500 mM NaCl
	20 mM Tris
Running buffer (1x)	192 mM Glycine

	0.1% SDS
	25 mM Tris
Sample buffer (Laemmli buffer 3x)	187.5 mM Tris (HCl) pH 6.8
	6% SDS
	30% Glycerol
	0.006% Bromophenolblue

2.1.4 Animal keeping

Food pellets, LASQCdiet Rod16 HiHy	Altomin	
Antifect N liquid	Schülke	#0297

2.1.5 Stereotactic injection

Fine forceps curved	Fine Science Tools	#11274-20
Disposable Scalpel	Braun	#01868278
Small scissors	Fine Science Tools	#14184-09
Bone scraper	Fine Science Tools	#10075-16
Needle Sterican 1.1 x 50 mm	Braun	#2057978
Needle Sterican 0.9 x 40 mm	Braun	#2050798
10 µl glass capillary/micropipette	Blaubrand intraMark	#708709
Silkam stitching silk	Braun	#C0761010
Needle Holders	Fine Science Tools	#12001-13
Eye salve	Bepanten	
Isoflurane CP	CP Pharma	
Ketamin 10%	Medistar	
Xylazin 20mg/ml	WDT	
Carprofen/Rimadyl	Zoetis	

2.1.5.1 Instruments

Stereotax	Kopf Instruments
Isoflurane system	EZ anesthesia
MiniVac Gas Evacuation Unit	Harvard Apparatus
Fluosorber Activated Charcoal Filter Canister	Harvard Apparatus
Heating plate/temperature control	FMC
Electric razor Aesculab	Isis
Dental drill Osada Success 40	Osada

Micropipette Puller P-1000	Sutter Instruments
MZ16 Microscope	Leica

2.1.6 Behavior

70% Ethanol	Honeywell	#UN1170
Wipes Soft wash cloth	Tork	#742200
Needle Sterican 0.9 x 40mm	Braun	#2050798
CNO Clozapine-N-oxide	Tocris Bioscience	#34233-69-7
Saline 0.9%	Braun	#2350720
Logitech Capture Camera	Logitech	

2.1.7 Perfusion

PBS tablets	Thermo Fischer Scientific	#18912014
4% PFA	Applichem	#141451.1211
Perfusion pump	Ismatec	
Needle Sterican 0.4 x 20 mm	Braun	#2050864
Big Scissors	Fine Science Tools	#14001-16
Small scissors	Fine Science Tools	#14060-09
Forceps rounded	Fine Science Tools	#11002-16
Bone cutting forceps	Fine Science Tools	#16152-11
Spatula	Fischer Scientific	#10269120
Plastic tray	VWR	#HECH42000016

2.1.8 Immunohistochemistry

PBS tablets	Thermo Fischer Scientific	#18912014
Triton X-100	Roth	#3051.3
NGS	Sigma-Aldrich	#S26-100ML
Agarose	Roth	#2267.4
Razor blades	Wilkinson	#7000115z
Fine brush, size 0	VWR	#149-2120
Superfrost plus microscope slides	Thermo Scientific	#J1800AMNZ
Cover slips 24x50 mm	Roth	#1871
Mowiol 4-88	Roth	#0713.1
Tweezers, flat tip	Fine Science Tools	#11073-10

2.1.9 Plastic ware

BD Falcon Primaria 6-well plate	Falcon	#353846
BD Falcon Primaria 24-well plate	Falcon	#353047
TPP® tissue culture dishes, 150x20 mm	Sigma-Aldrich	#Z707694-100EA
Cellstar tissue culture flask filter cap, 25 cm^2	Greiner bio-one	#82051-074
Microtube 0.5 ml safe-seal	Sarstedt	#72.699
Microtube 1.5 ml safe-seal	Sarstedt	#72.706.400
Microtube 2.0 ml safe-seal	Sarstedt	#72.695.400
Pipette tips, 200-1000 µl	Sarstedt	#70.762
Pipette tips, 20-200 µl	Sarstedt	#70.760.002
Pipette tips, 1-10 µl	Sarstedt	#70.1130
Filter tips, SafeSeal tips professional, 1000 µl	Biozym	#770400
Filter tips, SafeSeal tips professional, 200 µl	Biozym	#770100
Filter tips, SafeSeal tips professional, 20 µl	Biozym	#770050
Filter tips, SafeSeal tips professional, 10 µl	Biozym	#770010
Cellstar serological pipette, 25 ml	Greiner bio-one	#P7865
Cellstar serological pipette, 10 ml	Greiner bio-one	#P7740
Cellstar serological pipette, 5 ml	Greiner bio-one	#P7615
PP-tube sterile 15 ml	Sarstedt	#62.554.001
PP-tube sterile 50 ml	Sarstedt	#55.476.001
Gloves Semper care	Sempermed	#823781043
50 ml Syringe with luer lock	BD Falcon	#10636531
5 ml Syringe with luer lock	Braun	#10221742
3 ml Syringe with luer lock	Braun	#10703047
1 ml Syringe with luer lock	BD Falcon	#10630694
100 mm Petridish	Sigma-Aldrich	#P5731
60 mm Petridish	Sigma-Aldrich	#P5481

2.1.10 Laboratory Equipment

Water Bath Jubalo U3	Kurt Migge Laborbedarf
Heat Block QBA1	Grant
Shaking Heat Block Thermo-Shaker	Universal Labortechnik
37°C heating chamber	Memmert
37°C shaker	Edmund Bühler GMbH
Table Centrifuge Pico17	Thermo Fischer Scientific

Big Centrifuge MF-48-R	Awel centrifugation
Protein Gel Chamber	Bio-Rad
Voltage generator	Bio-Rad
Syringe Pump	Kd Scientific
Vibratome VT1000-S	Leica
Shaker Rocker 2D	Ika
Fluorescent Microscope Eclipse E-200	Nikon
Epifluorescent Microscope CTR6 LED	Leica
Confocal Microscope TCS SP5-II	Leica
Scale	Kern C-W
Fine scale ALC	Aculab
Magnet Stirrer D-6010	NeoLab
4°C Refrigerator	Liebherr
-20°C Refrigerator	Liebherr
-80°C Refrigerator Ultra low freezer U701	B medical systems
Microwave	Panasonic

2.2 Methods

2.2.1 Cell culture

The human embryonic kidney 293T (HEK293T) cell line was cultured and used for AAV production described in the following sections. HEK293T cells are derived from human embryonic kidney cells. Unfreezing and culturing of cells is described in the following paragraphs. All work was carried out in sterile conditions under the cell culture hood.

HEK293T cell stock was kept frozen in liquid nitrogen. For culturing DMEM with 4.5 g/l glucose, L-glutamine and without sodium pyruvate was used. Before use, 10% of fetal bovine serum (FBS) and 1% of penicillin/streptomycin (P/S) were added. This medium is later referred to as DMEM++. A small cell culture flask (75 cm^2) with a yellow screw cap with filter was filled with 15 ml of pre-warmed medium and put into the incubator (37°C with 5% CO_2). One vial of cells (usually 1 ml) was taken from liquid nitrogen and unfrozen in the hand. Unfrozen cells were then transferred into the prepared cell culture flasks and kept in the incubator. On the next day, the medium was changed. 24 h to 48 h later cells could be split into several big cell culture flasks (175 cm^2) with a red screw cap according to their density.

HEK293T cells are fast growing adherent cells and had to be split twice a week, approximately 1/10. Before splitting all solutions were pre-warmed in a water bath heated to 37°C. For splitting, first, supernatant was discarded, and cells were washed with 5 ml of PBS to remove dead cells and medium. Then, supernatant was removed and 2 ml of 0.5% Trypsin-EDTA were added per flask. After 1-2 min cells had detached from the bottom or were further detached by rapping on the side of the flask. Then, 8 ml of medium were added to stop the trypsinization. To split the cells, a part of the cell suspension, usually 1/10 of one flask, was diluted with medium to a total volume of 27 ml, transferred into a new cell culture flask and put into the incubator.

2.2.2 DNA preparation

For virus production, different plasmid desoxyribonucleic acid (DNAs) are necessary (see next section). Before starting with AAV production, the amount of stored DNA needed to be checked and more DNA needed to be produced if necessary.

2.2.2.1 Transformation

The first step in producing DNA consisted of transforming the plasmid DNA into competent bacterial cells (i.e. DH5 alpha E.coli strain).

Competent bacterial cells were taken from the -80°C freezer and kept on ice for 5 min. 1 µl of DNA was added to the competent cells and kept on ice for another 5 min. The bacteria were then heat-shocked for 30 sec at 42°C which allowed them to take up the DNA. Subsequently, the aliquot was put on ice shortly. 250 µl of SOC-medium were added to the competent cells and they were grown for 1 h at 37°C. Afterwards, 50 µl of bacteria containing medium were plated onto a LB-Agar plate containing Ampicillin. Bacteria were grown over night at 37°C.

2.2.2.2 Maxi preparation

To obtain DNA amounts of up to 1 mg (1 ml with a concentration of up to 1 µg/µl) HiSpeed Plasmid Maxi Kit from Qiagen was used.

To prepare for Maxi preparation, 150-200 ml of liquid autoclaved 2YT-medium were filled into baffled flasks. An autoclaved pipette tip was used to puncture a single bacterial culture from the LB-Agar plate and dropped into the flask. Then the bacteria in the liquid culture were grown over night at 37°C on a shaking platform at 125 revolutions per minute (rpm).

The next day Maxi preparation was conducted according to the manufacturer's protocol. Overnight culture was pelleted by centrifugation at 4500 rpm for 15 min. Medium was discarded, and the bacterial pellet was resuspended in 10 ml of resuspension buffer P1. For

lysis of the bacterial cells, 10 ml of lysis buffer P2 were added. The tube was inverted 4-6 times to mix and incubated at room temperature (RT) for 5 min. After the incubation, the lysis was stopped by adding 10 ml of neutralization buffer P3 and mixing by inverting. The lysate was poured into the closed QIAfilter Cartridge and incubated at RT for another 10 min. During the incubation, a HiSpeed Tip was equilibrated using 10 ml of equilibration buffer QBT. The QIAfilter Cartridge was opened, and the lysate was filtered into the HiSpeed Tip where the DNA bound to the resin filter. After a washing step using 60 ml of washing buffer QC, the DNA was eluted into a falcon tube with 15 ml of elution buffer QF. 10.5 ml of isopropanol were added to the eluate and mixed to precipitate the DNA. The mixture was incubated for 5 min. Following the incubation, the mixture was transferred into a syringe with an attached QIAprecipitator and filtered through the precipitator. This allowed the DNA to bind to the precipitator membrane. Subsequently, 2 ml of 70% ethanol were used to wash the membrane before it was dried by pressing air through the precipitator. Then, 1 ml of TE buffer was pipetted into a new syringe attached to the precipitator and the DNA was eluted into a collection tube. The elution step was repeated using the eluate to increase the DNA concentration. The DNA concentration was measured using a Nano Drop and the DNA was stored frozen at -20°C until further use.

2.2.3 AAV production

A helper plasmid-based system was used to enable production of AAV containing the desired DNA for subsequent protein expression in target cells. For the production HEK293T cells were used.

The week before AAV production, cells were split into 5 new flasks as explained in the cell culture section.

1st Day: Cells from the 5 flasks were detached as usual and collected in one of the flasks in 52ml of DMEM++. Then all cells were distributed equally onto 16 cell culture plates (3.5 ml of cells per plate), DMEM++ was added to a total amount of 20 ml and plates were placed back into the incubator.

3rd Day: Cells were transfected with plasmid DNA for virus production.

1 h before the transfection, 50% of the medium were substituted with new DMEM++ under sterile conditions. Sterile water and 2xHBS were pre-warmed to 37°C. For transfection 8 plates were used per virus, thus generally two different viruses could be produced at the same time.

Additional to the desired virus DNA, three helper plasmid DNAs were necessary for virus production. The helper plasmid H179 contained the adeno virus genes mediating AAV

replication. The helper plasmids H180 and H181 contained the Rep and Cap genes, relevant for proteins for the AAV life cycle and the capsid protein to produce chimeric serotype 1/2 AAV. A DNA mixture was prepared using 25 µg of helper plasmid H179, 6.25 µg of helper plasmids H180 and H181, and 13 µg of the DNA plasmid that should be integrated into the AAV. Each of these amounts was used per plate, thus, per virus amounts were multiplied by 8 and volume was adjusted according to plasmid DNA concentration. The total volume of the DNA mix was adjusted to 800 µl with nuclease-free water.

All further steps were carried out under sterile conditions. Per virus one transfection mix was prepared in a falcon using 6 ml of sterile water, 800 µl of DNA mixture and 1.2 ml of $CaCl_2$. 8 ml of 2xHBS were added to the transfection mix and mixed by inverting the falcon 4-5 times. After an incubation period of 3 min at RT, 2 ml of transfection mix were added dropwise to each plate. Plates were swayed gently and put back into the incubator.

5-6 h after transfection the medium was completely replaced by new DMEM++.

5th Day: 48 h after transfection cells were harvested. Medium was discarded and 10 ml of cold PBS were added per plate. Then cells were scraped using a cell scraper and collected in two falcon tubes per virus. To pellet the cells, tubes were centrifuged for 10 min at 1000 rpm. Supernatant was discarded. Cell pellets were resuspended in 45 ml of 150 mM NaCl 20 mM Tris puffer at pH 8.0 and directly frozen at -80°C to break the cell membrane open.

2.2.4 AAV purification

The next step in the AAV production process was digestion of the cell suspension. The suspension was unfrozen at RT. For lysis, 6.6 µl of Benzonase and 2.25 ml of 10% NaDoc were added to the suspension, and it was digested at 37°C for 1 h. During the incubation, the suspension was inverted every 10 min to improve digestion. Subsequently, the cell lysate was centrifuged for 15 min at 3900 rpm. After centrifugation, the supernatant was transferred into a new falcon tube and frozen at -80°C. The pellet was discarded.

On the next day, the virus purification was performed. The cell lysate was again unfrozen at RT and centrifuged at 3900 rpm for 15 min.

During centrifugation, two Heparin columns, 1 column per virus, were attached to a 50 ml syringe and equilibrated with 10 ml of 150 mM NaCl 20 mM Tris buffer at pH 8.0 using a syringe pump at a speed of 1 ml/min. Subsequently, the virus containing supernatant was loaded. During the flow through the column, the virus was bound to the heparin residues due to the serotype 2 parts of its capsid. For the first washing step, 20 ml of 100 mM NaCl 20 mM Tris

buffer pH 8.0 were used. Both steps were also performed using the syringe pump at the same speed as before.

The following washing and elution steps were then done by hand using a 5 ml syringe. The column was first washed with 1 ml of 200 mM NaCl 20 mM Tris buffer at pH 8.0 and then washed with 1 ml of 300 mM NaCl 20 mM Tris buffer at pH 8.0.

Then, three elution steps followed. Virus containing solution was collected in a 15 ml falcon. For the first elution step 1.5 ml of 400 mM NaCl 20 mM Tris buffer at pH 8.0 were used. This was followed by elution with 3 ml of 450 mM NaCl 20 mM Tris buffer at pH 8.0 and 1.5 ml of 500 mM NaCl 20 mM Tris buffer at pH 8.0.

To concentrate the virus, Amicon Ultra centrifugation filter columns were used. Virus eluate was loaded onto the column and centrifuged at 3200 rpm for 2 min. Flow through was discarded and virus was washed by filling the column with 1xPBS and centrifugation as before. This was repeated twice more. Approximately 250 µl to 500 µl remained in the column and were filled up with the same amount of PBS. Then, the virus solution was filtered into a 1.5 ml collection tube using a 0.2 µm Acrodisc column.

To control the success of virus production, a protein gel was prepared. Loading buffer was prepared by adding 46 µl of water and 6 µl of Mercaptoethanol to 46 µl of sample buffer. 10 µl of the prepared loading buffer were added to 5 µl and 10 µl of virus respectively. As a positive control already tested virus was used. Aliquots were held at 72°C for 10 min. Then virus samples and a protein marker were loaded onto a precast protein gel and run at 35 milli Ampere for 1 h in 1x running buffer. Protein gel was stained using Comassie blue stain reagent according to manufacturer's protocol. After staining only 3 bands – VP1, VP2, VP3 – should be visible.

After confirming successful virus production, virus was aliquoted in 10 ml aliquots and frozen until use at -80°C.

2.2.5 Animal keeping

For animal experiments and anatomical analysis, oxytocin receptor IRES-Cre knock-in rats (OTR-IRES-Cre rats) and WT rats from the same line were used. Rats used were female, 8 weeks old at the start of experiments and belonging to Sprague Dawley rat strain. OTR-IRES-Cre rats were generated by Prof. Dr. Dusan Bartsch at ZI Mannheim. As shown in Figure 5, in this knock-in rat model the Cre gene was inserted into one allele of the oxytocin receptor locus. The animals were kept as heterozygous in all presented experiments performed under approval by ethic committee (G-102/17, G-193/20). In total, I used n=8 wild type rats for

tracing study, n=13 OTR-IRES-Cre rats for anatomy of cell types and slice physiology, n=14 OTR-IRES-CRE rats for chemogenetic behavioral experiments, and n=14 OTR-IRES-Cre rats for ablation behavioral experiments.

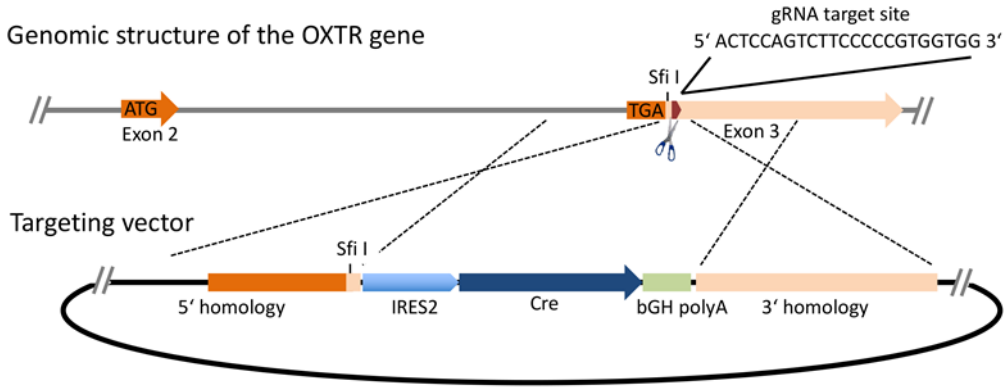

Figure 5: Schema of OTR-IRES-Cre knock-in rat. Using the Crispr/Cas9 method the IRES-Cre gene was inserted into the OTR gene locus of Sprague Dawley rats.

All animals were hosted in groups of 3-4 animals per cage and housed on a 12 h light-dark cycle with light phase between 6 a.m. and 6 p.m. with free access water and chaw.

2.2.6 Stereotactic injection

Prior to AAV injections into the hypothalamus or the hippocampus, rats received intra peritonal (i.p.) injection of a mix of ketamin (100 mg/kg body weight) and xylazin (5 mg/kg body weight). For AAV injections into the MEC, narcosis was induced by inhalation of 2-3% isoflurane to ensure a long and stable narcosis. For preoperative analgesia I used subcutaneous injection of 0.1 ml of carprofen.

The animal was positioned into the stereotactic frame, the head was shaved, and the eyes were covered with eye salve. The skin was cut with a scalpel and opened to the sides. The periost was numbed with a few drops of lidocaine solution. Then, a dental drill was used to open a small hole in the bone at the stereotactic coordinates for the injection site (see Table 1). Due to its location and structure, MEC injection deviated slightly from the general injection procedure and is explained in detail in the next paragraph. For the injection, a few microliters of virus solution were aspirated into a fine glass capillary, which was subsequently lowered into the prepared hole. The depth was dependent on the location of the desired structure (see Table 1). A small volume of virus 0.1-0.3 µl per injection site (see Table 1) was infused very slowly and afterwards the capillary was left in position for 3 min to prevent the spread of virus along the capillary tract. This procedure was repeated for each injection site.

Table 1: Coordinates for stereotactic injection

Brain region	Bregma	M/L	DV	Volume/site
PVN	-1.8	±0.35	-8.0	300nl
SON	-1.0	±1.8	-9.25	300nl
AN	-2.0	±1.2	-8.5	150nl
MEC	-10.0	±4.3 to 4.6	-8.0 to -5.0	150nl
Hippocampus CA1	-3.0	±2.0	-3.0	500nl
Hippocampus CA1	-4.0	±3.0	-2.8	500nl
MS	-0.8	±0.8	-7.4 to -7.0	300nl

As the MEC is located in the rostral part of the brain, directly in front of the cerebellum and elongated from ventral to dorsal along an angle (Figure 6A), location of injection site and process deviated from general injection procedure. To locate the injection site, the coordinates in Table 1 were used for the general location, but the specific injection site was chosen according to anatomical features described in Figure 6B in each animal. A hole was drilled at the chosen injection site, but the glass capillary was lowered into the hole at an angle of 20° to mimic the progression of the cortex. It was lowered to the deepest injection point and the volume indicated in Table 1 was injected. After keeping the capillary at the site for 2 min, it was retracted to 1 µm above the last injection site and a second injection was done. This was repeated until the last site, indicated in Table 1, was infused. For the MEC, I used 4 injection sites along the length of the cortex.

When the injections were finished, the holes in the bone were closed and the wound was stitched using sterile thread. Animals were kept in a cage on a plate heated to 38°C until they woke and then transferred into their home cage. For 48 h after surgery, animals were treated with carprofen once a day to reduce pain.

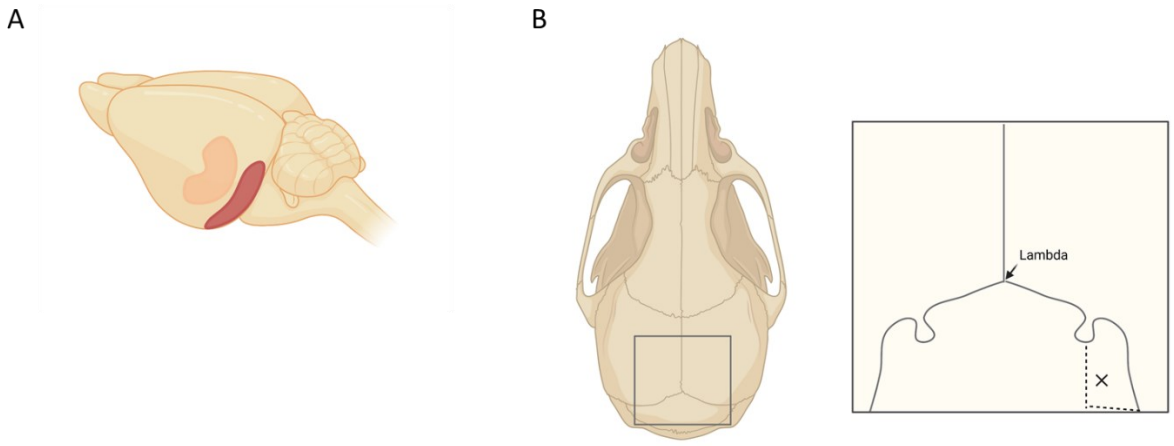

Figure 6: MEC injection. (A) MEC location in the brain. Created with BioRender.com (B) Specific location of MEC injection site is determined according to the skull fissures indicated in the drawing. Drilling location for MEC injection is indicated with a cross. Created with BioRender.com

2.2.6.1 FLP-FRT AAV system

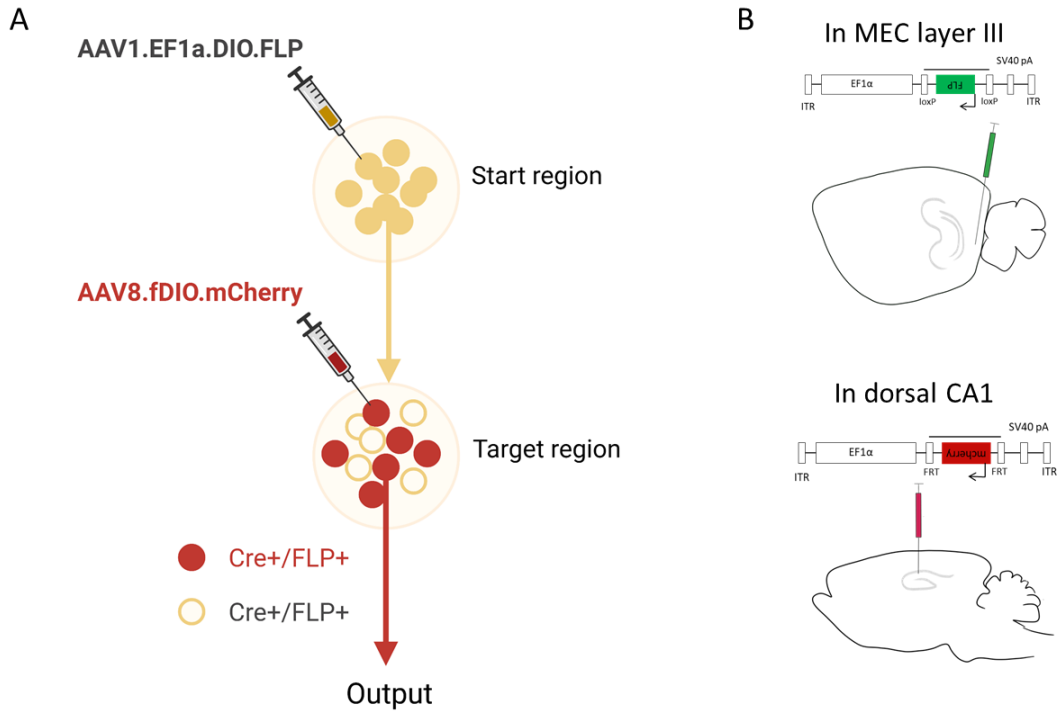

Figure 7: FLP-FRT AAV system. (A) Strategy for labeling Cre+ subpopulations of neurons in a target region receiving direct input from neurons in the start region (based on [94]). Created with BioRender.com (B) FLP-FRT AAV system used for injections in OTR-IRES-Cre rats. Cre-dependent FLP expressing AAV serotype 1 was injected in MEC layer III. FLP-dependent mCherry expressing AAV was injected in dorsal CA1.

Recombinase flippase (FLP) – short flippase recognition target (FRT) is a virus system using the FLP recombinase to anterogradely label the cell post-synaptic to the starter cell [94]. Starter AAV of serotype 1, which Cre-dependently expressed FLP and GFP under the control of ubiquitous promoter EF1a, was injected in MEC. In contrast to other AAV serotypes, single

AAV serotype 1 virions were then transported through the axon to the synapse and taken up by the post-synaptic neuron [94]. In addition, FLP-dependent mCherry expressing AAV of serotype 8 was injected in the post-synaptic region of interest, which was the dorsal hippocampus. This second virus acts as an amplifier for the fluorescent signal, as the few virions transported over the synapse usually do not lead to expression of detectable levels of fluorescent protein [94]. In my PhD thesis, I used a Cre-dependent version of FLP-expressing AAV and injected the viruses in an OTR-IRES-Cre female rat. Therefore, only post-synaptic OTR+ neurons in the dorsal hippocampus were labeled.

2.2.7 Behavior

To analyze the role of OTR+ neurons in the MEC, I performed a battery of behavioral tests on OTR-IRES-Cre adult female rats. The animals were divided into two groups and received injections of control AAV (EF1a_DIO_mcherry or EF1a_DIO_EGFP) or test AAV (EF1a_DIO_Gi_mcherry or EF1a_DIO_Caspase3) accordingly. In the chemogenetic experiments, both groups received intraperitoneal (i.p.) injections of CNO 40 min prior to the behavioral tests. Rats of both groups were group-housed in cages of two experimental Cre-positive rats with one none injected Cre-negative littermate. Additionally, novel Cre-negative stimulus adult female rats of the same age were introduced into tests involving social behaviors. The work was performed on female rats to exclude aggressive components of behaviors, typical for adult unfamiliar male rats.

2.2.7.1 Exploratory behavior

To investigate exploratory and anxiety related behavior, I used an open field test in which rats were placed into the center area of the open field and allowed to explore freely for 5 min. The videos were analyzed for exploratory behaviors such as the running path (distance and velocity) as well as anxiety related behaviors such as time spend in the center area using the Noldus EthoVision software.

2.2.7.2 Social interaction and social memory

The same arena was also used to analyze social interaction and social memory.

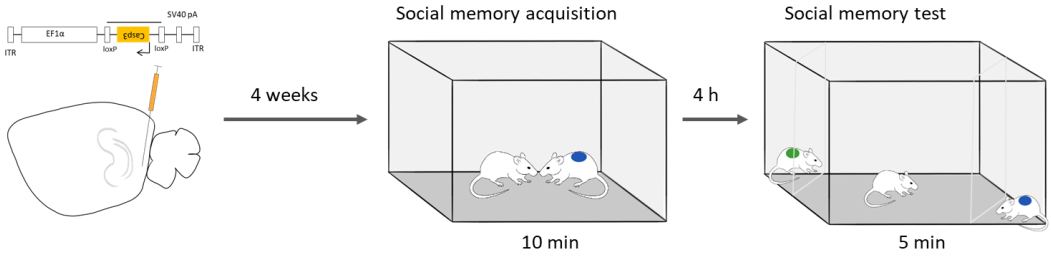

Figure 8: Paradigm used to test social memory. Approximately 4 weeks after virus injection, after prior habituation to the open field, animals were allowed to freely interact for 10 min with a novel animal (indicated by blue spot on its back). 4 h after the interaction, test animals were placed in the open field again. The stimulus animal from the previous interaction was placed behind a Plexiglas with holes in one corner, while the other corner contained a novel stimulus animal. Test animals were allowed to explore for 5 min and a video was recorded for further manual analysis.

Figure 8 displays the paradigm that was used for social memory behavior. In the morning, animals were allowed to freely interact with a novel stimulus animal for 10 min. 4 h later social memory was tested. For this, the open field was slightly modified so two corners were separated by transparent Plexiglas panels with holes to allow direct nose to nose interaction. The familiar stimulus animal, known from the interaction in the morning, was placed in one corner of the open field, while the unknown conspecific was placed in the opposite corner. The test animal was placed in the open field and allowed to explore and interact for 5 min. In the Gi experiment, both groups of test animals received an injection of 3 mg per KG body weight of CNO 40 min prior either the interaction in the morning or before the social memory test in the afternoon. This paradigm was slightly modified for Caspase experiments. In the modified setup interaction time was increased to 20 min and the test was performed 1 h after interaction. Also, the Plexiglas was replaced with metal mesh to enable more direct interaction.

Video material from social interaction in the morning was analyzed for changes in social behavior by measuring time and amount of general interaction and different social behaviors such as sniffing, mounting and following.

For the social memory test, the time spent in direct interaction/close proximity in a pre-defined area was measured. Additionally, the Track Rodent Software [95] was used to analyze interaction time in more detail including the duration of the interaction bouts and the interaction times over the course of the test.

2.2.7.3 Reward learning

Reward learning was done in the T-Maze. Animals were habituated in the empty T-Maze for 2 days with 5 trial runs each day. On the following day, reward learning started. For social reward learning, the stimulus littermate from the same cage was placed in the arm, that the animals visited less often during habituation, behind a Plexiglas wall with holes enabling

sniffing and nose-to-nose interaction. As a comparison, reward learning was repeated with a food reward in one corner, which consisted of small chocolate flakes, after an extinction and second habituation period. A visual cue was placed at the entry of the same arm (see Figure 9). Each test animal had 5 choice runs per day. A choice run consisted of placing the test animal in the start area. After a period of 10 sec, the barrier was lifted to give access to the T-Maze. The animal was allowed to choose freely which arm to enter and left in the arm for 10 sec or until it turned and started running into another direction. An auditorial cue (a beep) was sounded before the animal was taken out of the T-Maze to reduce stress to the animal and prevent the rat from reacting to other noises (like movement or rustling of a lab coat). The rat was placed back into the start area for the next run or put back into the home cage.

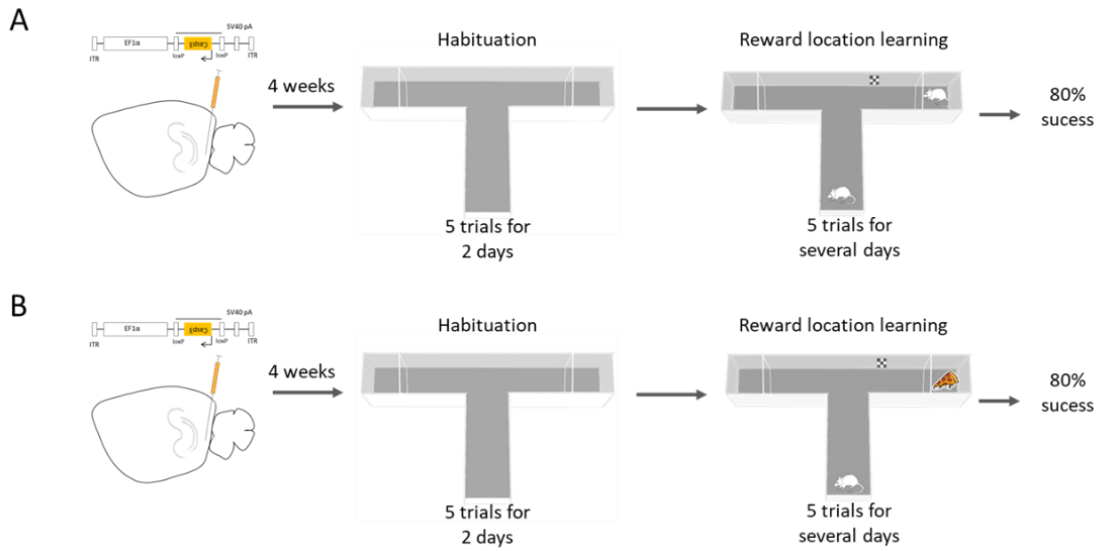

Figure 9: T-Maze reward learning paradigms. Approximately 4 weeks after virus injection T-Maze reward learning started. During 2 days of habituation test animals had 5 trial runs in the empty T-Maze. For the reward learning (A) a conspecific animal as a social partner or (B) a food reward was placed in the reward arm for each of the 5 runs. Reward learning was done for 10 days.

For each animal the choices were calculated as percentage of trials the animal chose the arm containing its littermate/the food reward and plotted as a learning curve over the consecutive days.

In the Gi experiments, once the animals reached a level of choosing the reward arm in 70% of trials at average, they were injected with 3 mg per KG body weight of CNO. After 40 min animals were tested for 3 choice runs in the T-Maze without a social partner.

2.2.8 Perfusion

3 weeks after stereotactic injection or after behavior experiments, animals were perfused transcardially using 4% paraformaldehyde (PFA) to preserve the tissue and allow safe extraction of the brains for anatomical analysis.

To prepare perfusion, a tubing system was attached to the perfusion pump. The system consisted of two tubes going either into PBS or 4% PFA solution which were connected by a valve to the outgoing tube that had a needle attached at the end. The valve allowed switching between PBS and PFA. To prepare, PFA was pumped into the tubes until the valve, then PBS was pumped until it started dripping out of the needle. It was important to make sure that no air bubbles remained in the tubing system.

Animals were first anesthetized, then killed with an overdose of isoflurane. Directly after death occurred, the animal was put on a Styrofoam plate and its legs were fixed. The thorax was opened to expose the heart and the needle was inserted into the left ventricle. The right atrium was cut and the pump was started. PBS was pumped into the left ventricle at a speed of 60 ml/min until the liver paled. Then the valve was switched to pump PFA into the body. When the PFA-induced seizures stopped, the pumping speed was lowered to 30 ml/min until approximately 200 ml of PFA were used. Stiffness of the neck and extremities was checked to evaluate success of the procedure.

After stopping the perfusion, the head was separated from the body. The skin and muscle were cut away. Pliers were used to break the skull and pull away the pieces to expose the brain. After the bones were discarded, a spatula was used to lift the brain up out of the skull from the front. The optic and trigeminal nerves were cut, and brain completely freed from the skull. The brain was transferred into 4% PFA and kept overnight at 4°C for proper fixation. Then the PFA was changed for PBS for longer storage, or the brain was sliced for analysis.

2.2.9 Immunohistochemistry

Sectioning of the brain was performed on the Leica VT1000-S vibratom. The anterior parts of the brain including hypothalamus regions and dorsal hippocampus were sectioned in coronal 50 µm sections while the MEC was sectioned in 40 µm sagittal sections.

Before sectioning, the brain was cut using a template to make a coronal cut posterior to the dorsal hippocampus. The anterior part was then embedded into 3% agarose with the coronal plane down. The posterior part was cut along the middle into the two hemispheres. The cut surface was placed on a thin slice of agarose and then embedded into agarose. For sectioning, a razor blade was cut into two pieces and fixed into the vibratom holder. The container was

filled with PBS. The embedded brain piece was glued to the specimen holder in the desired orientation and then fixed in the PBS filled container. The slices were cut at a frequency of 9-10 and a speed of 6-8 according to the tissue. Slices were collected either in a 6-well plate with PBS for subsequent staining or in glass vials filled with cryoprotector to be stored at -20°C.

Before staining, sections were washed 3x with PBS. Then, sections were put into 5% NGS in 1% Triton-PBS for 30 min on a shaker to block unspecific bindings. Subsequently, sections were incubated for 24-72 h on a shaker at 4°C in the designated combination of primary antibodies prepared in 1% Triton-PBS. A maximum of three antibodies binding to three different target proteins could be combined as long as their host species was different. After incubation, slices were washed 3x with PBS. Subsequently, sliced were incubated for 2 h on a shaker at RT in the corresponding secondary antibody, which bound to the primary antibody and was labeled with a fluorescent dye. Primary and secondary antibodies and their dilutions used are listed in Table 2.

Table 2: Antibodies and their dilutions

Primary antibody	Final dilution	Secondary antibody	Final dilution
Mouse anti-OT	1:2000	Goat-anti mouse Cy3 or Alexa680	1:500 or 1:1000
Mouse anti-NeuN	1:3000	Goat-anti mouse Alexa680	1:1000
Chicken anti-GFP	1:10000	Goat-anti chicken Alexa488	1:1000
Rabbit anti-dsRed	1:1000	Goat-anti rabbit Cy3 or Alexa594	1:500 or 1:1000
Mouse anti-RFP	1:1000	Goat-anti mouse Cy3 or Alexa594	1:500 or 1:1000
Rabbit anti-PCP4	1:1000	Goat-anti rabbit Cy3 or Alexa647	1:500 or 1:1000
Rabbit anti- PV	1:1000	Goat-anti rabbit Alexa647	1:1000
Mouse anti-GAD67	1:1000	Goat-anti mouse Alexa 680	1:1000

Images were taken on either the epifluorescent microscope CTR6 LED from Leica or the confocal microscope TCS Sp5-II from Leica. The epifluorescent microscope was used mainly for overview pictures of a slice or region stitched from multiple images, while the confocal microscope was used for high quality and high resolution images of fine morphology of cells and their processes.

2.2.10 Statistical analysis

Data are presented as mean ± standard error of the mean (SEM). The statistics program GraphPad Prism v5.01 was used for graphical presentation and statistical analysis. In addition,

R was used for graphical presentation of box plots. Multiple data points were compared using two-way Anova with Bonferroni's multiple comparison test as a specific post-test. Data of only two samples were analyzed with T-test.

Statistically significant difference was considered as $p>0.05$.

3. Results

3.1 Anatomy of OT projections to MEC

To enable OT signaling in the MEC, it is first important to verify that OT axons innervate this structure and, thus, can release the neuropeptide there. Therefore, first I analyzed axonal projections from OT neurons of the hypothalamus to the MEC.

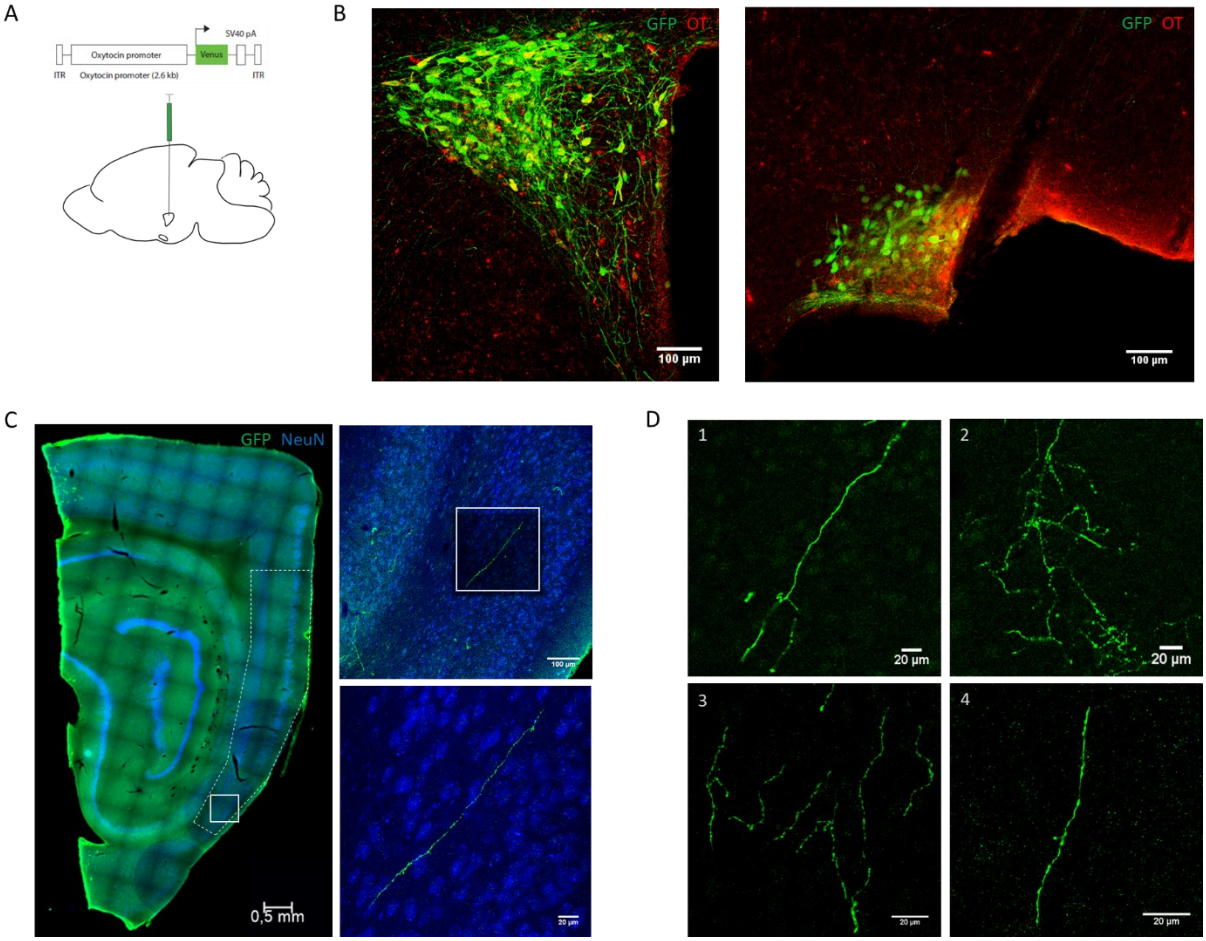

Figure 10: Axonal projections from OT neurons. (A) Schema of injection of OTpromoter_Venus AAV into PVN and SON of the hypothalamus. (B) Expression of Venus in the hypothalamus is restricted to OT neurons. Staining for green fluorescent protein (GFP) (green) and OT (red). (C) Axonal projections from OT neurons to the MEC. Fibers can be found in different parts of MEC. Most prominent fibers are located in layer III. Immunostaining for GFP (green) and Hexaribonucleotide binding protein 3 (NeuN) (blue). (D) Examples of magnified OT axons in the MEC. Staining for GFP in green.

As depicted in Figure 9A, AAV expressing Venus driven by OT promoter was injected in the SON and PVN of a wildtype adult female rat. Due to cell type specificity of the promoter, Venus expression was restricted to OT neurons as was verified by immunostaining for GFP and OT (Figure 10B). Projections from infected OT neurons to the MEC are shown in Figure 9C. Most

dense projections were found traversing through layer III, although scattered Venus-positive axons were detected in all layers. Following injections in PVN or SON only, projections in MEC were present in both cases indicating that both PVN and SON neurons send axons to MEC (data not shown).

3.2 Anatomy of OTR+ neurons in the MEC

3.2.1 General anatomy

OTR+ neurons were labeled by AAV equipped with Cre-dependent green fluorescent protein (GFP) driven by generic EF1α promoter injected into the MEC of adult female OTR-IRES-Cre rats (Figure 11A).

As shown in Figure 11B the injection was restricted to the MEC region. OTR+ neurons were present along the dorso-ventral axis of the cortex. In the dorsal part, OTR+ neurons were predominantly located in layer III. In the ventral MEC, layer III also contained most OTR+ neurons, but there was also a higher number of neurons present in layer II.

Counting of OTR+ neurons was conducted in 3 different brains using slices from both hemispheres and counting one ventral and one dorsal 10x image per slice. Of the cells in MEC about 15% were OTR+. 92% of positive neurons were located in layer III. Of the remaining 8% about 5% of neurons were located in layer II. If only layer III was analyzed, up to 65% (mean 46% ± 2%, n=6) of all layer III neurons expressed OTR.

OTR+ neurons were counted in layer III (mean = 230 ± 12; up to 330, n=6) both in dorsal and ventral part of MEC. For layer II and layer V number of OTR+ neurons were different between dorsal and ventral MEC with only about 5-20 cells per layer in dorsal MEC but up to 50 cells per layer in ventral MEC.

Per slice 12.5 ± 1 inhibitory neurons were identified using GAD67 immunostaining. In contrast, counting of excitatory cells, marked by PCP4 in layer III, determined a number of 167 ± 9 cells per slice. As a result, 93% of OTR+ MEC neurons were identified as excitatory neurons while 7% were inhibitory neurons.

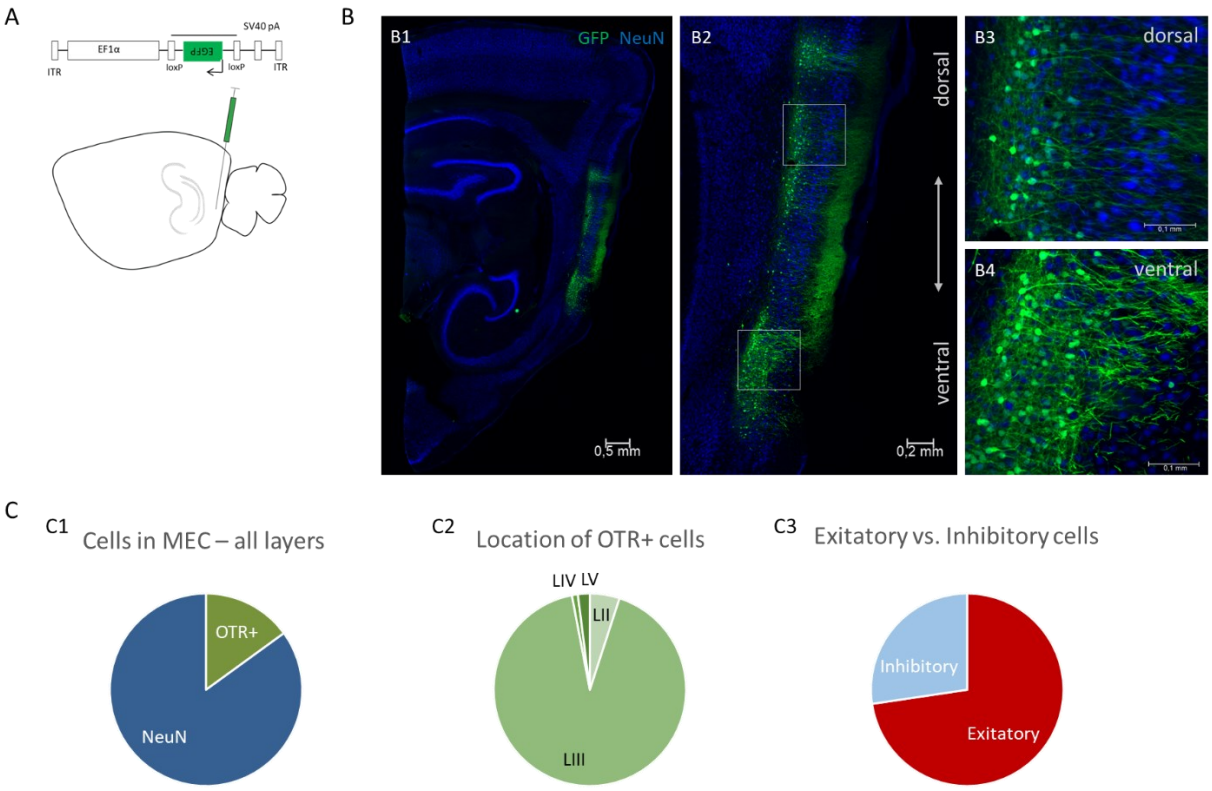

Figure 11: OTR+ neurons in the MEC. (A) Schema of injection of Cre-dependent EGFP expressing AAV along the dorso-ventral axis of the MEC. (B) (B1) Overview of a sagittal slice with EFGP labeled OTR+ cells only in MEC. (B2) Shows the expression of EGFP in OTR+ cells along the dorso-ventral axis of MEC. Magnified images depict phenotypes of OTR+ cells in dorsal (B3) and ventral (B4) portions of MEC. Staining for GFP (green) and NeuN (blue). (C) OTR+ cell numbers in the MEC. OTR+ cells and NeuN stained cells were counted in all layers in one ventral and one dorsal 10x image per sagittal brain slice. Shown are (C1) the percentage of OTR+ cells of all neurons n=3, (C2) the distribution of the OTR+ cells in the different layers of the dorsal MEC n=7 and (C3) the percentage of excitatory vs. inhibitory OTR+ neurons n=3.

3.2.2 Cell types

To further analyze OTR+ cell types in MEC, slices containing OTR+ cells were counterstained by antibodies against GFP and antibodies against Purkinje cell protein 4 (PCP4), parvalbumin (PV) and GAD67 (Figure 12).

OTR+ layer III neurons were verified as excitatory pyramid cells positive for PCP4 as shown in Figure 12A. Layer III neurons showed typical pyramid phenotype with a triangular shaped soma and a long apical dendrite traversing layer II. Basically, all layer III pyramid neurons that expressed GFP also expressed PCP4.

In contrast, neurons in layer II and in layer V were mainly cells expressing markers typical for GABA-ergic neurons, such as GAD67 and PV (Figure 12B and 12C). A few interneuron-like cells were also located in layer III.

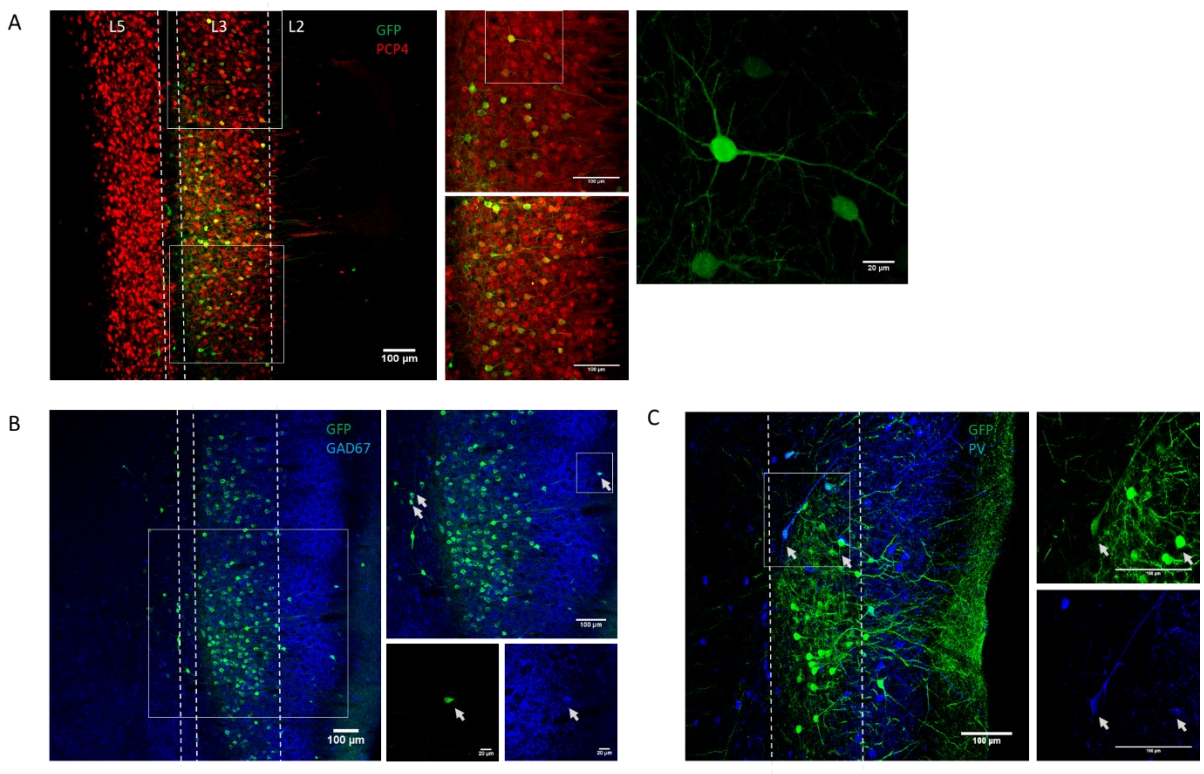

Figure 12: OTR-expressing cell types in the MEC. (A) Immunostaining with PCP4 (red) and GFP (green) antibodies revealed that nearly all green OTR-positive neurons in layer III expressed PCP4, a marker of principle cells. (B) Immunostaining for GFP (green) and the GABA-ergic neuronal marker GAD67 (blue). Arrows indicate cells with colocalization of GFP and GAD67 immunosignals in layer II and layer V. (C) Immunostaining for PV (blue) and GFP (green) identifies some double positive neurons (arrows) in layer II and layer III.

3.2.3 Long range projections of OTR+ MEC neurons

To study extra-MEC projections of OTR+ neurons, I analyzed forebrains of OTR-IRES-Cre female rats, injected with Cre-Dependent AAV expressing GFP (Figure 11).

As shown in Figure 13A (left panel A1), a strong plexus of GFP expressing fibers from OTR+ neurons of the MEC was found in the *stratum lacunosum-moleculare* (SLM) of the dorsal hippocampus with single fibers to the dorsal CA1 *stratum pyramidale* (SP). In addition, I identified projections to the hippocampus along the alvear pathway (Figure 13 panel A2). Axons traversing along the alvear path were less dense than the plexus in SLM, but fibers from the alvear path as well as from the plexus in SLM traversed to SP (Figure 13 panel A3).

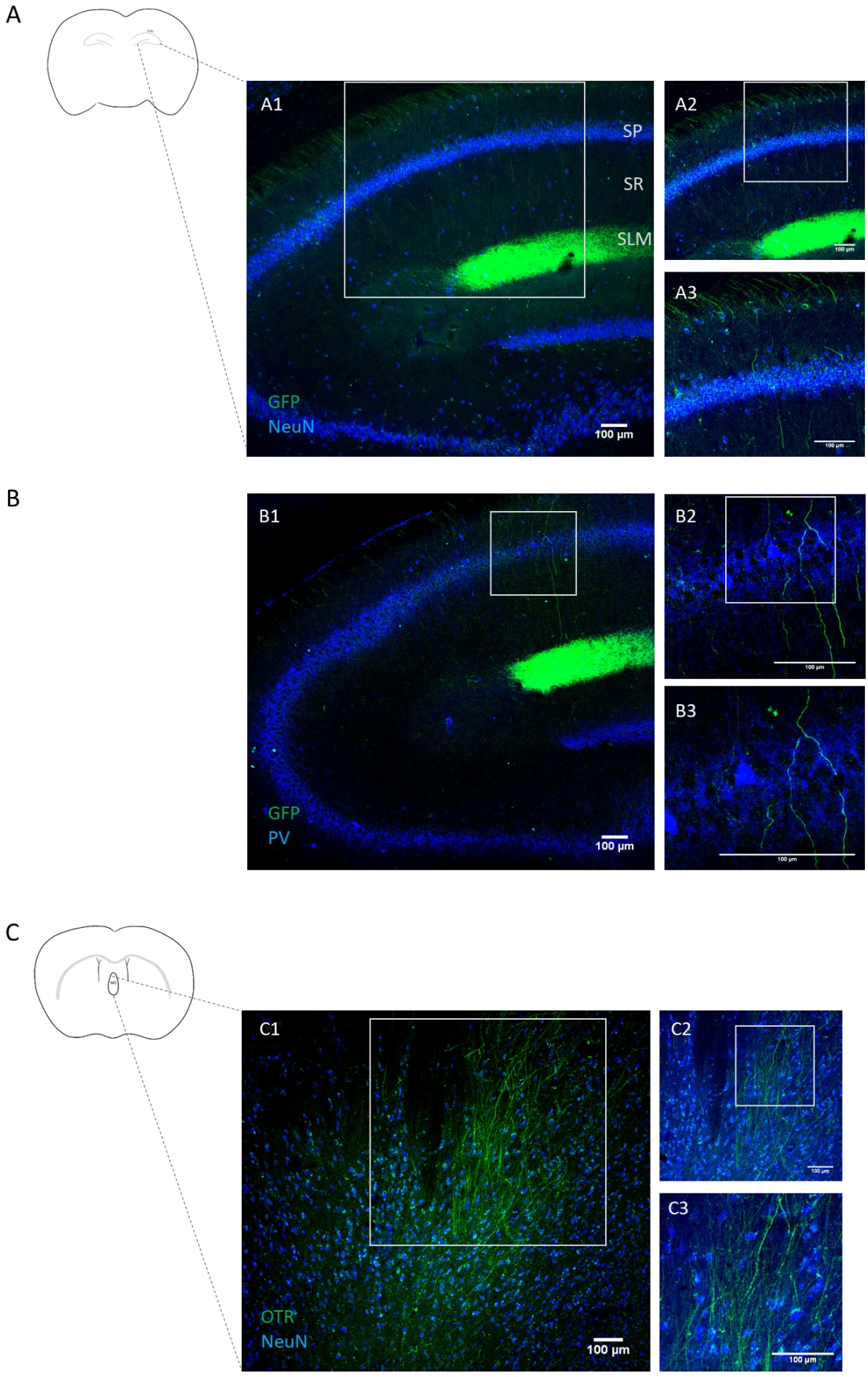

Figure 13: Axonal projections of OTR+ neurons of the MEC. (A) OTR+ MEC neurons project towards the dorsal hippocampus. Immunostaining for GFP (green) in axons of OTR+MEC neurons and NeuN (blue) for

hippocampal neurons. (B) Axonal projections of OTR+ MEC neurons were located in close proximity to PV+ interneurons in dorsal CA1. Immunostaining for GFP (green) in axons of OTR+MEC neurons and PV (blue) for hippocampal interneurons. (C) OTR+ MEC neuron projections to the MS. GFP staining (green) and NeuN staining (blue).

Axons of OTR+ MEC neurons, that traversed to CA1 SP layer, were found in close proximity to PV+ CA1 interneurons (Figure 13B).

Additionally, projections in medial septum (MS) were found (Figure 13C), which is a region known to be involved in theta rhythm regulation in the hippocampal structure. Fibers were more numerous in posterior MS (shown in Figure 13C) than anterior MS (not shown).

3.2.4 Monosynaptic tracing from the MEC towards OTR+ neurons in the dorsal hippocampus

To tackle the question whether MEC projections terminate onto OTR+ neurons of the dorsal hippocampus, I employed Cre-dependent FLP and GFP expressing AAV of serotype 1, which was injected in MEC layer III. A second AAV expressing mCherry in a FLP-dependent manner was injected in dorsal hippocampus CA1 region to label local OTR-Cre neurons postsynaptic to starter cells in the MEC (Figure 14A).

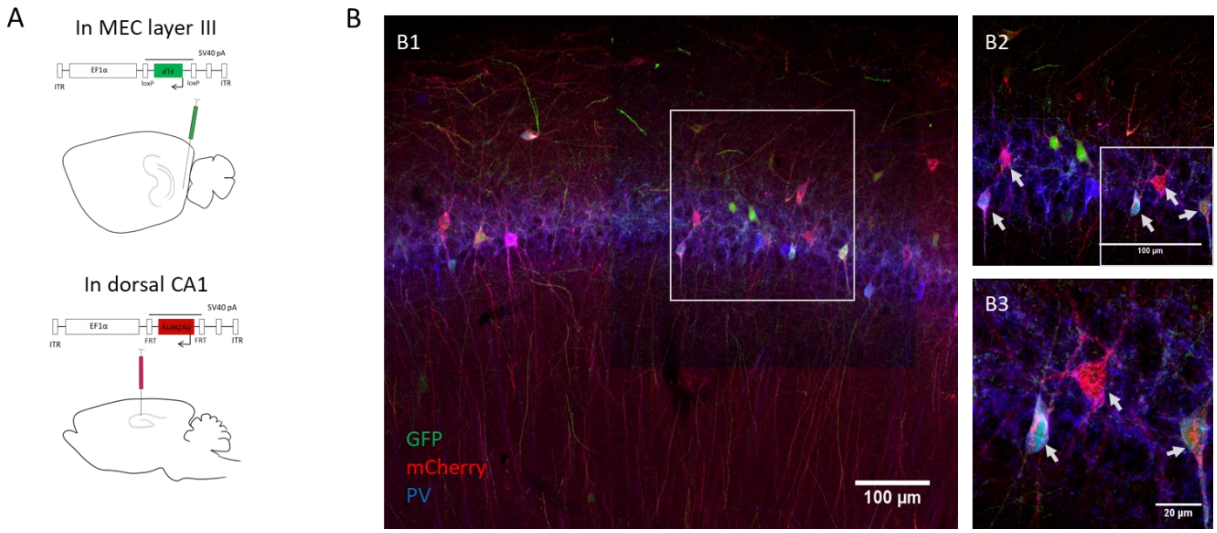

Figure 14: Labeling of OTR-expressing post-synaptic cells in dorsal CA1. (A) FLP-FRT AAV system. Cre-dependent FLP expressing AAV serotype 1 was injected in MEC layer III. FLP-dependent mCherry expressing AAV was injected in dorsal CA1. (B) Putative post-synaptic OTR-expressing cells in the dorsal CA1 express interneuronal marker parvalbumin (PV). Immunostaining for GFP (green), mCherry (red) and PV (blue). PV positive neurons that at least also express mCherry are marked with an arrow.

In the dorsal hippocampus a number of putative post-synaptic OTR+ cells have been labeled in red, indicating that these particular cells are CA1 OTR-expressing neurons (Figure 14B).

Most of identified OTR+ cells exhibited morphology of interneurons and were positive for parvalbumin (Figure 14 panel B2 and B3), suggesting that they belong to PV-positive basket interneurons of CA1.

3.3 Behavior

3.3.1 Chemogenetic silencing of MEC OTR+ neurons

3.3.1.1 Social interaction

To analyze social interest and social interaction behaviors in general, I performed a pilot experiment placing animals in the open field together with an unfamiliar female conspecific of the same age and allowed them to freely interact for 5 min.

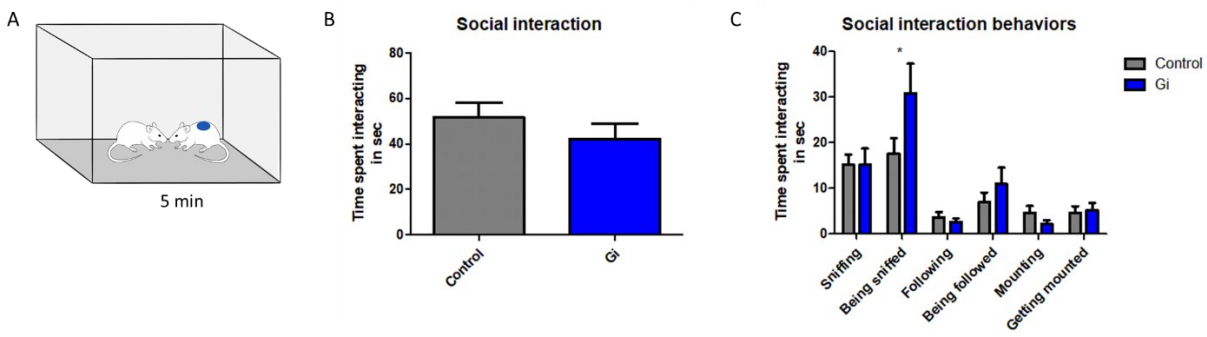

Figure 15: Social interaction in Gi vs control group. (A) Drawing of free social interaction in the Open Field. Experimental rat (white) is interacting with novel stimulus rat (blue). (B) Cumulative time spent interacting of the test rat (Gi or control group) with the stimulus rat. Interaction time was measured in seconds. Statistical analysis using T-test showed no significant differences between groups. (C) Interaction time was divided into different social interaction behaviors. Time spent performing each type of behavior was measured in seconds. Statistical analysis using 2-way Anova showed a significant difference between groups only in time being sniffed. N=6

The analysis of videos revealed that there were no significant differences between "Gi" (e.g. with chemogenetically silenced OTR+ MEC cells) and control group in the cumulative time spent interacting with the novel stimulus animal. From the analyzed components of social interaction only the time the stimulus animal spent sniffing was significantly increased in the Gi group. All other behaviors were similar in both groups.

3.3.1.2 Social memory

To study the effect of OTR+ MEC cells on of social memory, rats were allowed to interact with a social conspecific for 10 min. 4 h later social memory was tested. Test rats were placed in

the open field with the social partner from the earlier interaction (familiar conspecific) confined to one corner and a new unknown conspecific in the other corner (Figure 16A). CNO was injected either 40 min before the social interaction to observe an effect on memory acquisition or 40 min before the social memory test to investigate memory retrieval.

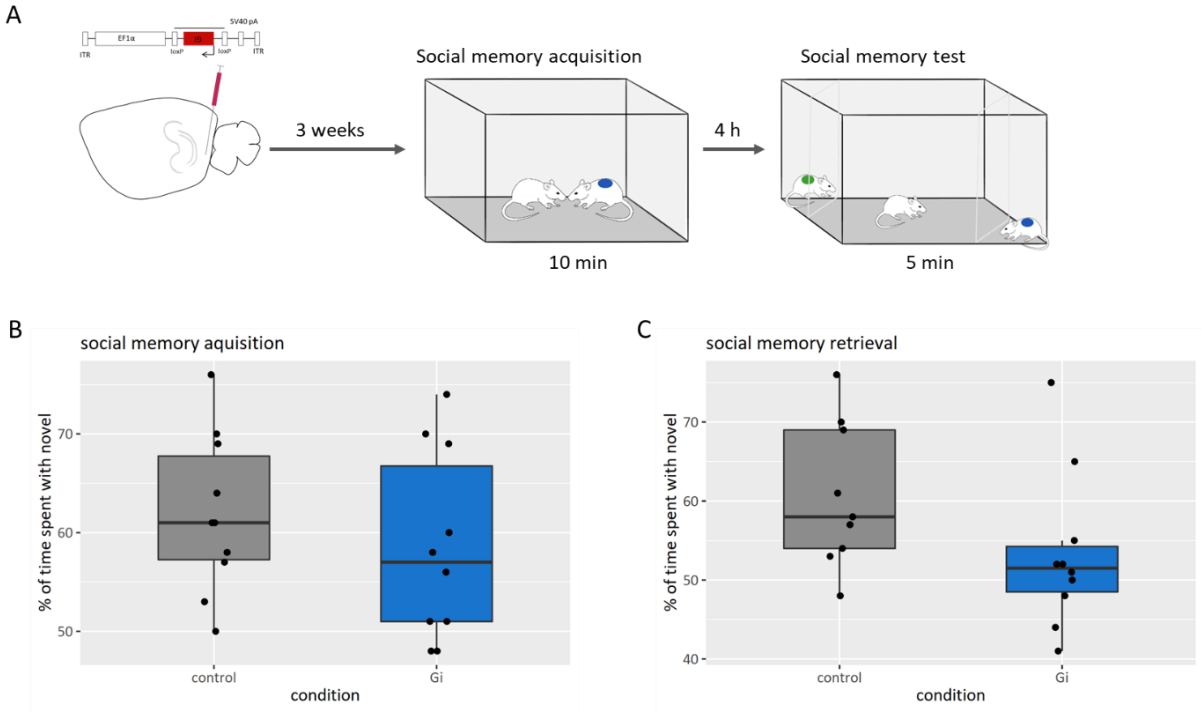

Figure 16: Social memory test in Gi vs. control animals. (A) Schema of social memory test. After virus expression, animals had 10 min of free social interaction with an unknown conspecific rat (marked blue) for social memory acquisition. 4 h later, the conspecific rat from morning (rat is marked by blue spot) was presented in one corner and a new conspecific (marked green) was presented in the opposite corner both separated by mesh. Test rats could move in the open field and interact with both conspecifics for 5 min. (B) Effect of Gi on social memory acquisition. CNO was applied to the test rat 40 min before the 10 min free social interaction to inhibit OTR+ neurons during memory acquisition period. Time spent interacting with the known rat and the novel rat was measured during the 5 min social memory test. The boxplot indicates the percentage of time spent interacting with the novel rat from the cumulative interaction time. The line in the middle depicts the mean and the dots represent each test rat. Analysis of the date using T-test identified no significant difference between groups. Control group: n=9 Gi group: n=10 (C) Effect of Gi on social memory retrieval. CNO was applied to the test rat 40 min before the 5 min social memory test to inhibit OTR+ neurons during memory retrieval period. Time spent interacting with the known rat and the novel rat was measured during the 5 min social memory test. The boxplot indicates the percentage of time spent interacting with the novel rat from the cumulative interaction time. The line in the middle depicts the mean and the dots represent each test rat. Analysis of the date using T-test identified no significant difference between groups. Control group: n=9 Gi group: n=10

No significant differences were found neither when OTR+ cells were inhibited in the social memory acquisition (Figure 16B) or retrieval phase (Figure 16C). In both experiments, interindividual differences between animals led to big variances in the data. However, there seemed to be a trend towards a loss of preference for interacting with the novel stimulus rat in the Gi group especially when CNO was applied to inhibit memory retrieval (Figure 16C).

3.3.1.3 T-Maze

The T-Maze was used to analyze navigation towards the location of a familiar conspecific. To train animals over 6 days, a conspecific rat was placed in one corner of the T-maze arm marked by a visual cue. Test rats were given 5 trial runs per day until they chose the social reward location with a mean of 70% success. The next day, rats were injected with CNO 40 min before the test.

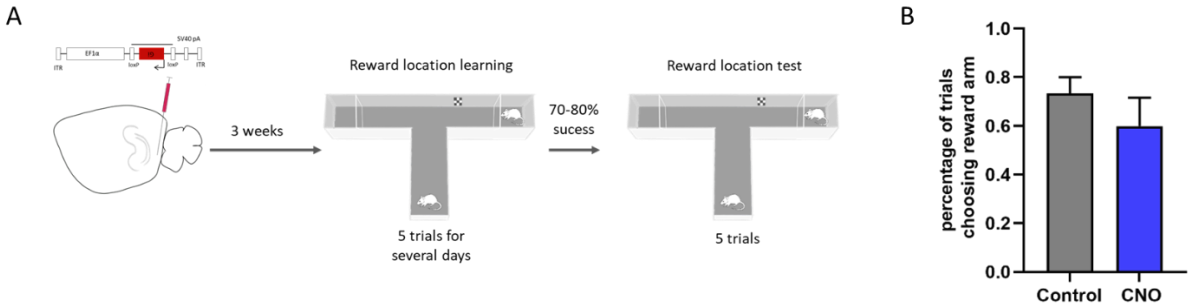

Figure 17: T-Maze test in Gi vs. control group. (A) Schema of T-Maze test. After AAV expression, rats had 5 trial runs in the T-maze per day with a littermate confined in one corner of the T-maze. The littermate was placed behind a Plexiglas with big holes, so animals could interact. A visual cue was placed at the start of the reward arm. When animals reached a mean level of choosing the reward arm 70% of the time or above, the reward location test was done on the next day. 40 min before testing, animals received a CNO injection to inhibit MEC OTR+ neurons during the reward location test. During the reward location test, T-Maze set up was identical to the learning period. (B) In the reward location test, the control column displays the proportion of trials the test rats choose the reward arm on the last day of the learning period. The CNO column shows the proportion of trials the test rats choose the reward arm after inhibition of OTR+ neurons in MEC during the reward location test. T-Test analysis resulted in no significant differences. N=3 per group

No significant change was shown between the proportion of choosing the social reward arm on the last day of the learning period and during recollection of the location of conspecific in the test while OTR+ MEC neurons were silenced by CNO.

3.3.2 Genetic ablation of OTR+ MEC neurons

As the chemogenetic-based experiments resulted in no significant results, despite low number of animals being used, I selected a different method to exclude OTR+ neurons in MEC prior to the start of the memory acquisition phase. Using Cre-dependent modified Caspase 3 AAV, OTR+ cells in the MEC were ablated. After expression of Caspase 3, inducing apoptosis of OTR+ cells, animals were subjected to the similar behavioral experiments with some slight modifications as described below.

3.3.2.1 Anatomical analysis

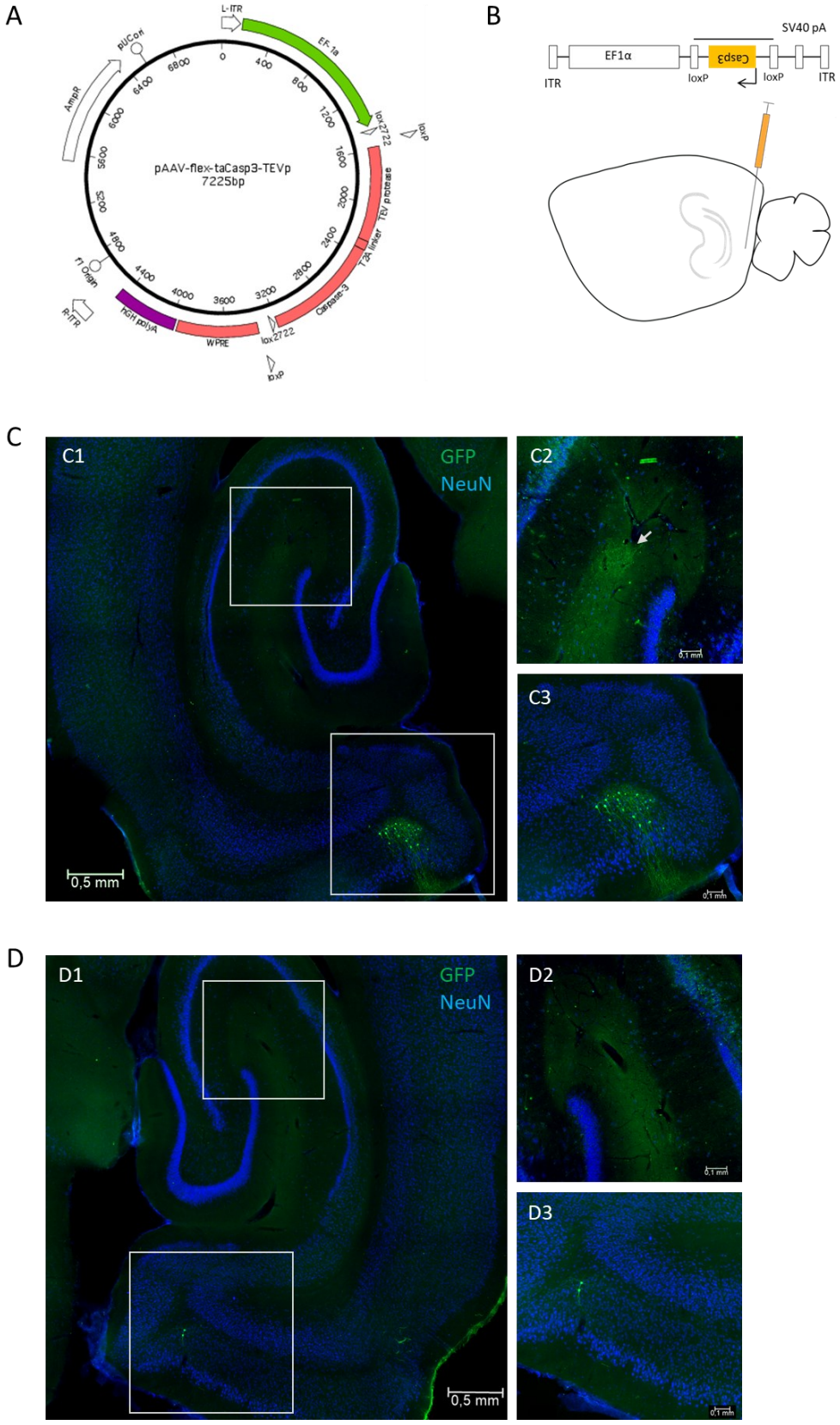

Figure 18: Injection of Cre-dependent Caspase 3 expressing AAV in the MEC. (A) Schema of AAV structure. AAV expression is driven by EF1a promoter. Modified Caspase 3 gene is inverted between two LoxP sites and followed by TEV protease gene separated by a T2A site. Upon entering Cre-expressing cells, Caspase

and TEV genes can be flipped and will be expressed. Modified Caspase is then cleaved by TEV protease into its active form, leading to apoptosis in the expressing cell. pAAV-flex-taCasp3-TEVp was a gift from Nirao Shah & Jim Wells (Addgene plasmid # 45580 ; http://n2t.net/addgene:45580 ; RRID:Addgene_45580) [96] (B) Schematic drawing of AAV injection along the dorso-ventral axis of the MEC. Control AAV Cre-dependently expressing EGFP diluted 1:3 with PBS was injected into the left hemisphere. In the right hemisphere 1/3rd control AAV was combined with 2/3rd Caspase AAV and injected in MEC. (C) Horizontal brain section of the left hemisphere injected with only control AAV leading to Cre-dependent expression of EFGP in OTR-expressing cells in MEC. GFP is stained in green, NeuN in stained in red. In the overview (C1) and in the lower magnified image (C3) green cells in MEC are shown. In the upper magnified image (C2) the white arrow marks green axons coming from MEC OTR+ neurons. (D) Horizontal brain section of the right hemisphere injected with 1/3rd control AAV combined with 2/3rd Caspase AAV. GFP is stained in green, NeuN in stained in red. In the overview (D1) and in the lower magnified image (D3) only two green cells were visible. In the upper magnified image (D2) no projections from MEC were visible in the hippocampus.

To verify that AAV driven Caspase 3 expression in OTR+ cells of the MEC was sufficient to ablate these cells, a separate animal was injected at the same time as the rats dedicated to behavioral experiments. This animal received the injection of a mix of $^1/_3$ Cre-dependent EGFP expressing AAV (100nl per site) and $^2/_3$ Cre-dependent AAV expressing modified Caspase 3 (200nl per site) in the right hemisphere. The same volumes of Cre-dependent Caspase 3 AAV were injected in rats dedicated to behavioral testing. In the left hemisphere, the animal was injected with a mix of $^1/_3$ Cre-dependent EGFP expressing AAV and $^2/_3$ PBS same as the control group. This animal was killed after 4 weeks and survival of OTR+ neurons in the MEC was histologically analyzed (Figure 18).

As shown in Figure 18C, there are EGFP expressing OTR+ neurons present in the left MEC, but almost no GFP expressing neurons could be found in the right MEC (Figure 18D). Additionally, while the hippocampus in the left hemisphere shows GFP labeled projections from MEC (Figure 18C2, indicated by arrow), no innervation of GFP stained axons was seen in the right hemisphere (Figure 18D2).

3.3.2.2 Open field

To test whether locomotor activity, investigative behavior and anxiety were not influenced in animals after ablation of OTR+ MEC neurons (named as “Caspase group”), rats were videotaped in open field. Movement track, velocity and distance as well as time in the center area were analyzed using Noldus EthoVision software.

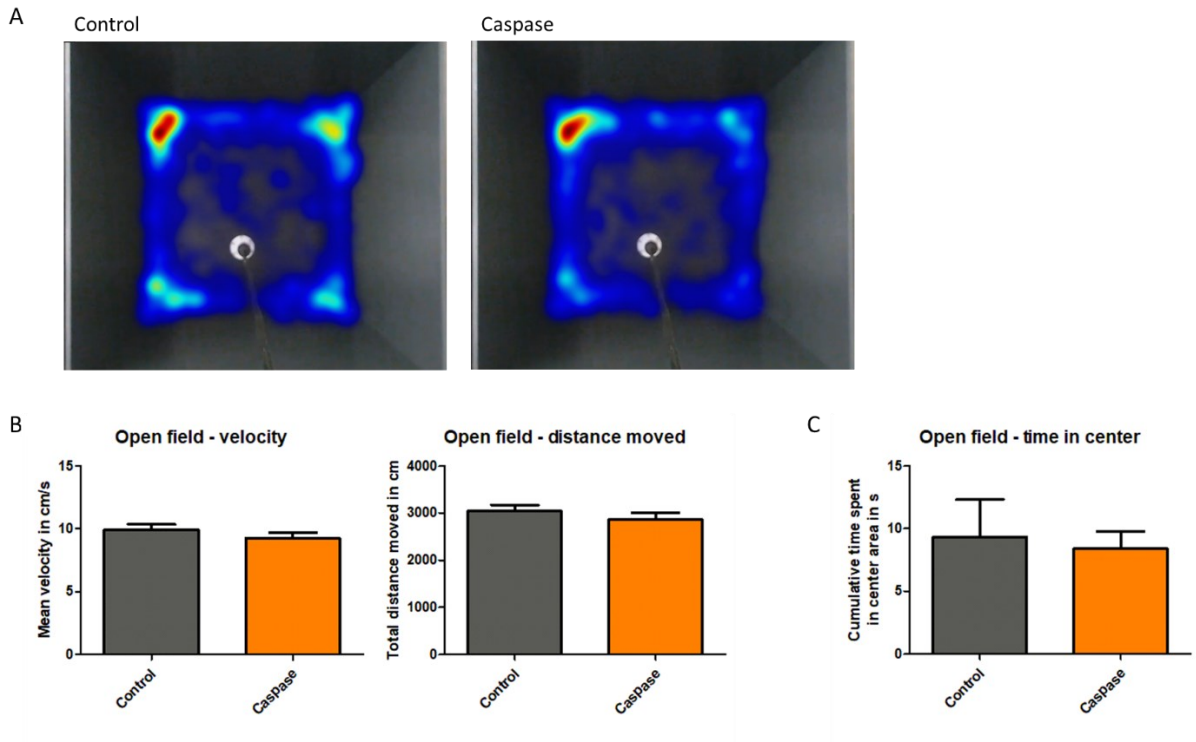

Figure 19: Locomotor activity, investigative and anxiety-like behavior after ablation OTR+ MEC neurons. (A) Heatmaps showing the movement of all animals sorted by group during the 5 min of free exploration in the open field. Control group heatmap is depicted on the left, Caspase group heatmap on the right. (B) Mean velocity and total distance moved were calculated for each animal from the tracked video files. Mean velocity in cm/s is shown on the left for both groups. The graph on the right shows the total distance moved in cm. Both graphs show group mean + SEM as error bars. (C) To estimate differences in anxiety levels, the time spent in the center area of the Open Field was analyzed. The cumulative time spent in the center is shown as mean + SEM for both groups. Control group n=5, Caspase group n=7

The analysis of behaviors revealed no differences between Caspase and control groups (Figure 19). Movement heatmaps have a similar appearance in both groups (Figure 19A). The velocity and distance moved during open field investigation were not significantly different (Figure 19B). Anxiety levels, as estimated by the time spent in the center area, were also similar in both groups (Figure 19C).

3.3.2.3 Social interaction

As first part of the social memory test paradigm, rats were allowed to interact freely. To test whether social interaction altered after ablation of OTR+ MEC neurons, the first 5 min of the free social interaction were analyzed for general social interaction time in Caspase group compared to controls.

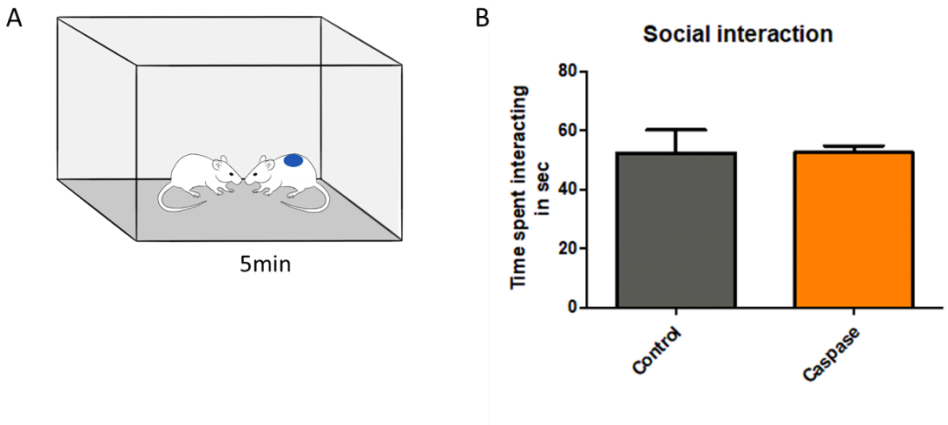

Figure 20: Social interaction of rats in Caspase vs. control group. (A) Drawing of free social interaction in the open field. Experimental rat is interacting with novel stimulus rat (marked by blue spot). (B) Cumulative time spent interacting of the test rat (Caspase or control group) with the stimulus rat. Interaction time was measured in seconds. Statistical analysis using T-test showed no significant differences between groups. Control group n=5, Caspase group n=7

The analysis revealed no significant differences in the time spent interacting with an unfamiliar conspecific between the Caspase and the control group.

3.3.2.4 Social memory

For the social memory test, the paradigm was slightly modified to enhance the preference in the control group (e.g. to increase their motivation to communicate with conspecifics). To achieve this, rats were isolated in single cages but kept in the same room for the night (16 h) before the experiment. The social interaction period was increased to 20 min to strengthen social memory, followed by 1 h break (Figure 21A).

In addition to the percentage of time spent with the novel conspecific from the complete interaction time (Figure 21B), for this experiment further parameters were analyzed such as the investigation of stimuli along time and length of the investigation bouts. This was done using the TrackRodent program [95].

The extra-analysis could show that with this setup, the control and caspase group rats had a trend to spent more time interacting with the novel conspecific compared to the familiar conspecific though this was not significant as interindividual differences in interaction time were pronounced (Figure 21C and D). Also, in the intermediate and long bouts this trend was especially prominent as shown previously by Netser et al, 2020 [95]. However, no significant differences were found between the control group and the caspase group analyzing the proportion of time spent interacting with the novel conspecific (Figure 21B).

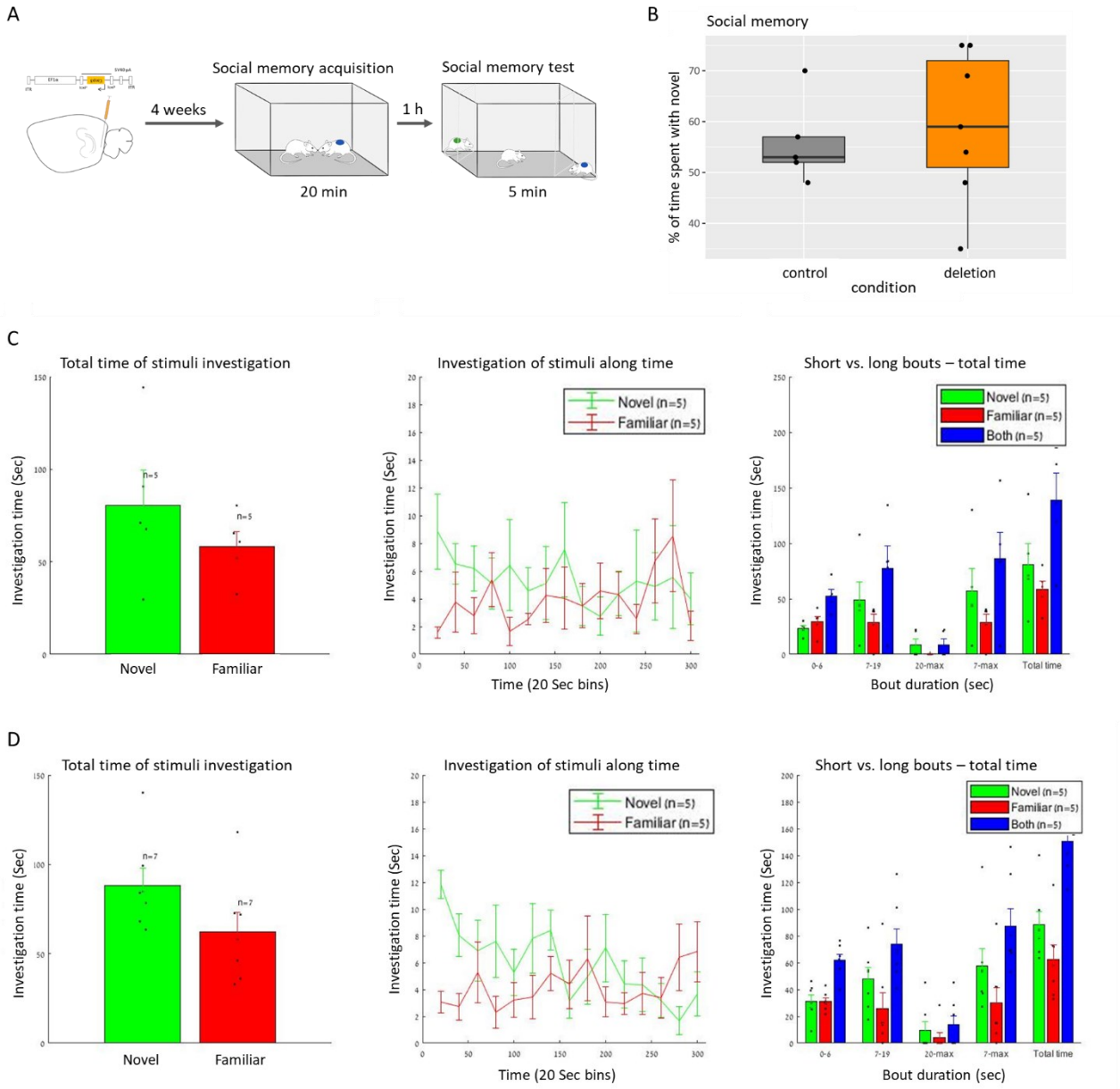

Figure 21: Social memory in Caspase vs. control group. (A) Schema of social memory test. After virus expression, animals had 20 min of free social interaction with an unknown conspecific rat (marked blue) for social memory acquisition. 1 h later, the conspecific rat from morning (blue) was presented in one corner and a new conspecific (green) was presented in the opposite corner both separated by mesh. Test rats could move in the open field and interact with both conspecifics for 5 min. (B) Effect of Caspase on social memory. Time spent interacting with the familiar rat and the novel rat was measured during the 5 min social memory test. The boxplot indicates the percentage of time spent interacting with the novel rat from the cumulative interaction time. The line in the middle depicts the mean and the dots represent each test rat. Analysis of the data using T-test identified no significant difference between groups. (C+D) Social interaction of control group rats (C) and Caspase group rats (D) during social memory test was analyzed using the TrackRodent program [95]. The graphic on the left shows absolute interaction times with the novel and the familiar conspecific. Data is depicted as mean + SEM, with dots for each animal. The plot in the middle shows the interaction time with the different conspecifics along time with a data point every twenty seconds. The final graphic divides the interaction into different bouts depending on the length of the interaction period. There are short bouts with 0-6 sec, intermediate bouts with 7-19 sec and long bouts with more than 20 sec. Control group n=5, Caspase group n=7

3.3.2.5 T-Maze

In contrast to the chemogenetic experiment where OTR+ neurons were only inhibited for a short time period (after 3 hours CNO is almost completely absent in plasma levels [97] and concentration is presumably under the threshold for DREADD receptor activation [98]), using Cre-dependent Caspase 3 AAV led to complete ablation of these cells. This allowed me to investigate the role of OTR+ MEC cells in the process of reward location learning in the T-Maze setup over several days. Besides, it was important to analyze if the Caspase group showed a general impairment in a reward location learning paradigm or if an impairment is specific to a social reward. Therefore, the T-Maze reward location test was performed using a social reward and after an extinction phase it was repeated with a food reward (Figure 22).

In the social reward learning paradigm, the learning curve of the Caspase group was located below the learning curve of the control group during the whole experiment. Although, single data points were not significantly different, fitted curves to the data showed a significant difference between the groups (Figure 22B). In contrast, there were no significant differences between groups in the food reward learning paradigm (Figure 22C). On the last day of the experiment, all groups exceeded the level of choosing the reward arm in 70% of trials except for the Caspase group in the social reward learning paradigm (Figure 22D). Furthermore, in the social reward learning 5/5 rats in the control group but only 2/7 rats in the Caspase group chose the reward arm in 80% of trials on at least 2 days. In the food reward learning all animals in both groups reached that level.

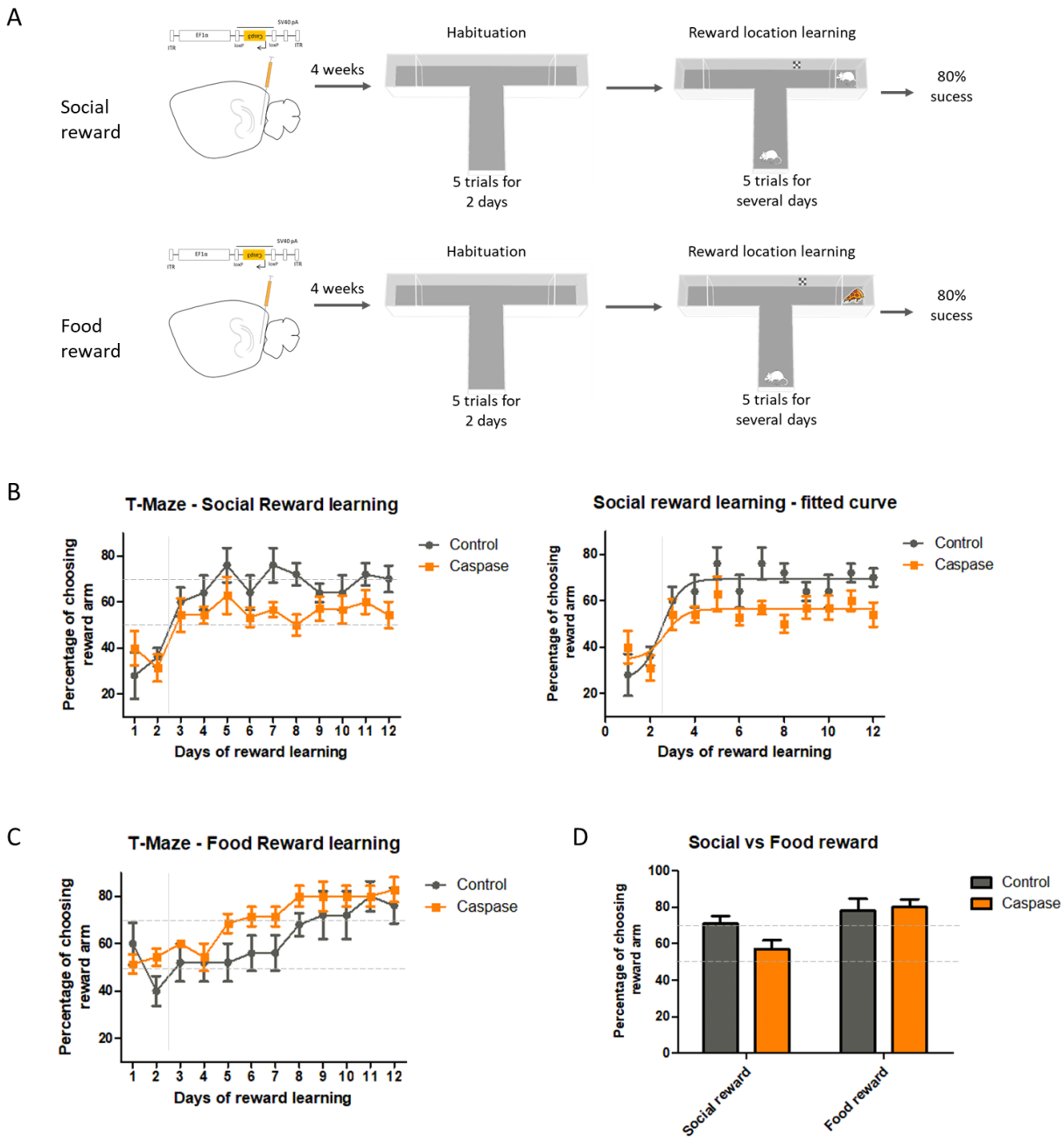

Figure 22: T-Maze test in Caspase vs. control group. (A) Schema of T-Maze test. After AAV expression, rats had 5 trial runs in the T-maze per day for 2 days in the empty T-Maze. After habituation a littermate for the social reward or chocolate pellets for the food reward were placed in one corner of the T-maze. The littermate was placed behind a Plexiglas with big holes, so animals could interact. A visual cue was placed at the start of the reward arm. Test rats had 5 trial runs per day for 10 consecutive days. (B) Social reward learning in the T-Maze. Proportion of trials choosing the reward arm is shown as mean percentage for each group per day ± SEM as error bars. Dashed lines mark the 50% and 70% level. Data was analyzed using 2-way Anova. No significant differences were found for the single days. In the right graph sigmoidal curves were calculated for both groups of data points. These curves were significantly different from each other, indicating a significant difference between the two data sets. (C) Food reward learning in the T-Maze. Proportion of trials choosing the reward arm is shown as mean percentage for each group per day ± SEM as error bars. Dashed lines mark the 50% and 70% level. Data was analyzed using 2-way Anova. No significant differences were found for the single days or when calculating fitted curves for the two groups of data. (D) Social reward vs food reward learning. Graph shows the mean proportion of trials choosing the reward arm in percent per group for the last day of reward learning. Dashed lines mark the 50% and 70% level. Data was analyzed using 2-way Anova. Control group n=5, Caspase group n=7

4. Discussion

The aim of this study was the investigation of anatomical connections of the OT system with the MEC-hippocampus domain as well as the functional relevance of this network. In this PhD thesis I showed that OT neurons innervate the MEC. OT axons were most prominently located in layer III of MEC. In conjunction, OTR-expressing neurons in MEC were predominantly located in layer III and exhibited an excitatory PC phenotype. Consistent with this, projections of OTR+ MEC neurons predominantly terminated in the ipsilateral dorsal hippocampus. Deletion of OTR+ MEC neurons led to impaired learning of a social reward location, but not a food reward location. These results suggest the involvement of rat OT-MEC-hippocampus pathway in the modulation of social navigation.

4.1 Hypothalamic OT neurons innervate the MEC

OT neurons are known to send axons to various brain regions including parts of the hippocampus complex, such as the ventral hippocampus and the lateral EC [45]. Here I also described axonal OT projections towards the MEC. Importantly, both main OT-ergic nuclei, the PVN and SON, predominantly project to MEC layer III with distinctive straight OT axons traversing through the layer.

Compared to the study of OT innervation of different forebrain regions [45], the innervation of MEC would probably be classified as low to intermediate. OT axons in MEC were not spread evenly over the whole cortex but in some slices, axons were accumulated in an area. Thus, taken over the whole MEC OT innervation is probably comparable to the one previously reported for lateral EC and in some areas to ventral hippocampus [45].

4.2 MEC neurons express OTRs

In this study, I identified OTR+ neurons using Cre-dependent expression of fluorescence proteins through virus injection in the target brain region of transgenic OTR-IRES-Cre knock-in rats. The OTR-IRES-Cre knock-in rat model is essential for the investigation of OTR+ cells in different brain areas as it not only allows for easy identification of those cells but also enables specific manipulation. Furthermore, other methods to identify OTR expression mostly depend on detecting OTR mRNA as a reliable antibody is currently not available [53]. Specificity of Cre expression in OTR-IRES-Cre knock-in rats has been verified using the *in situ* hybridization and RNAscope in different brain regions by our group (not published).

Taking advantage of this transgenic rat, OTR+ neurons were detected predominantly in layer III of MEC accounting for approximately half (up to 65%) of layer III cells, depending on strength of injection. They were spread along the dorso-ventral axis of the MEC with some changes in cell distribution towards ventral MEC, precisely, that the amount of interneurons in layer II and V was increased in ventral MEC.

Of the neurons expressing OTR in MEC, 93% were identified as excitatory PCs residing in layer III. These neurons expressed the layer III neuronal marker PCP4 and gave rise to strong projections to the dorsal hippocampus [17,18]. The second identified cell population were interneurons expressing the interneuronal marker Glutamate decarboxylase (GAD67) and mostly in layer II also PV. Interneurons expressing PV in layer II and III have been described before and are considered to be the interconnecting part between stellate cells [14,15].

Both identified OTR+ cell types were verified in our group by *ex vivo* electrophysiology (Figure 23). The electrophysiological characterization, done by Dr. Julia Lebedeva, confirmed my anatomical finding, demonstrating the existence of two types of OT-sensitive neurons in the MEC: PCs and fast-spiking interneurons (Figure 23A). Furthermore, bath application of selective OTR agonist TGOT led to firing in both pyramid neurons and fast-spiking interneurons expressing OTR (Figure 23B), thus, reinforcing the specificity of the OTR-IRES-Cre knock-in rat model.

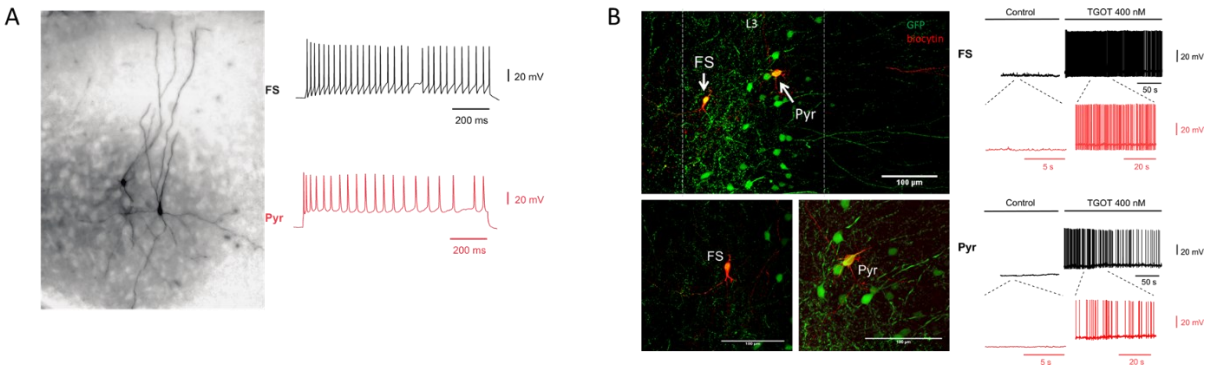

Figure 23: Electrophysiological properties of OTR-expressing neurons in MEC. (A) Brightfield image of biocytin labeled neurons in MEC and their electrophysiological profiles. The left neuron was identified as a fast-spiking interneuron (FS). The right neuron with pyramid phenotype also showed the electrophysiological profile of a pyramid neuron (Pyr). (B) OTR-expressing neurons are labeled with GFP in a horizontal brain slice. Patched neurons were filled with biocytin, stained in red, to identify them in the slice. Both biocytin filled neurons also express GFP. The slice was treated with selective OTR agonist TGOT and patched cells were recorded. On the right the firing patterns are shown during baseline and during TGOT application. The fast-spiking interneuron, which was located towards the border of layer III and V, showed strong increase in firing after application of TGOT. The pyramid neuron also started firing upon TGOT application. The electrophysiological characterization was performed by Dr. Julia Lebedeva.

Compared to several forebrain areas that have been previously or are currently investigated by our group, the composition of OTR-expressing cell types in the MEC is quite unique. For example, in the central amygdala OT innervation leads to activation of interneurons that are

part of a local inhibitory circuit [45]. OTR expression on interneurons has also been reported in other cortices such as the auditory cortex [99] and the prefrontal cortex [100]. Current studies on OT function in the infralimbic cortex or the insular cortex also display a different distribution of OTR-expressing cells with the main group of OTR+ neurons represented by multiple types of interneurons (unpublished results). Thus, composition of OTR-expressing cell types in the MEC consisting of 93% excitatory projecting neurons and only 7% interneurons is exceptional and can only be somewhat comparable to the ventral hippocampus (unpublished results).

4.2.1 OTR-expressing pyramid neurons in MEC layer III innervate hippocampus CA1 region

In line with literature [14,17], layer III OTR+ MEC neurons send strong projections to dorsal hippocampus. OTR+ MEC neuron projections traveled along the path described for EC layer III PCs to the SLM of dorsal hippocampus. From there single axons traversed towards the *stratum pyramidale*. Additionally, OTR+ axons also traversed along the previously described alvear path [35] to reach the dorsal CA1. GABA-ergic long-range projections from MEC layer II and III to dorsal hippocampus interneurons have also been reported, however, GABA-ergic interneurons only made up about 1% of all back-labeled cells projecting to hippocampus [101]. Therefore, OTR+ MEC neuron projections to dorsal CA1 can be expected to mainly emanate from layer III PCs.

The dorsal CA2 mainly receives input from EC layer II neurons [102]. Input from a few layer III MEC neurons to CA2 had been reported using retrograde tracing [103] but could not be confirmed in studies using genetic models [80,104]. Using PCP4 immunostaining to specifically label CA2 region [105], I did not find axons of OTR+ MEC cells in the dorsal CA2.

Innervation from MEC OTR+ cells was also found in medial septum. From literature it would be expected that innervation to extra-hippocampal structures arises from layer Va pyramid cells [14,19,20]. However, only single OTR+ neurons in layer V were observed. So far back-tracing experiments from the MS were not successful in identifying OTR+ neurons projecting there. In general, it is known that MS is connected to the hippocampus complex. For example, the MS-hippocampal pathway is crucially involved in Theta rhythm and regulates CA1 excitability [106] and MS innervates the MEC to coordinate local inhibitory networks [107]. The MEC to MS connections have been less investigated but might provide a feed-back circuit.

4.2.2 What is a cellular target of OTR+ MEC neurons in the CA1?

OTR+ MEC neuron projections to dorsal CA1 were found in close proximity to PV+ interneurons in *stratum pyramidale*. To further investigate postsynaptic cells in dorsal CA1, I employed the FLP-FRT system [94]. Although, this system does not allow to reconstruct anterograde transsynaptic projections from a OTR+/Cre MEC cell, it provided me with a possibility to identify CA1 cells putatively receiving input from non-selectively labeled neurons of the MEC.

In this study, I found that layer III MEC neurons innervate post-synaptic OTR-expressing neurons in dorsal CA1 region. Interestingly, a lot of the post-synaptic neurons expressed GFP as well as mCherry. As usually too few virions get transported over the synapse to allow detection without enhancing the signal by employing the second FLP-dependent virus [94], this leads to the conclusion that several virions were transferred into the post-synaptic neurons to trigger GFP expression strong enough for detection. A reason for this might be that axons from several different MEC layer III neurons terminate on the same hippocampal interneuron. This might also explain the relatively low number of post-synaptic neurons detected in the dorsal hippocampus. Besides, only OTR-expressing post-synaptic neurons were visible, so an additional number of OTR-negative post-synaptic neurons might be also visualized.

The labeled post-synaptic neurons had mainly interneuronal phenotypes and were predominantly located in the *stratum pyramidale* and *stratum orients*. Staining for the interneuronal marker PV revealed expression in post-synaptic neurons in the *stratum pyramidale*. Labeled PV-positive cells can represent local basket cells, which are known to form inhibitory synapses onto multiple CA1 PCs [33]. Additionally, singular post-synaptic neurons had the anatomical appearance of pyramid neurons, function of which remained to be determined.

Even though the FLP expressing virus can enter all cells in MEC, innervation of the dorsal hippocampus CA1 region is known to be restricted to MEC layer III neurons [30,32,34] and of these neurons approximately 50% were shown to express OTR. Thus, it is tempting to propose that layer III OTR+ neurons of the MEC contribute to the innervation of dorsal CA1 interneurons. Intriguingly, OTR+ MEC neurons potentially innervate other OTR+ CA1 neurons, implying that OT sensitive pathways in different regions are connected to generate a coordinated response to release OT in one or both structures [108].

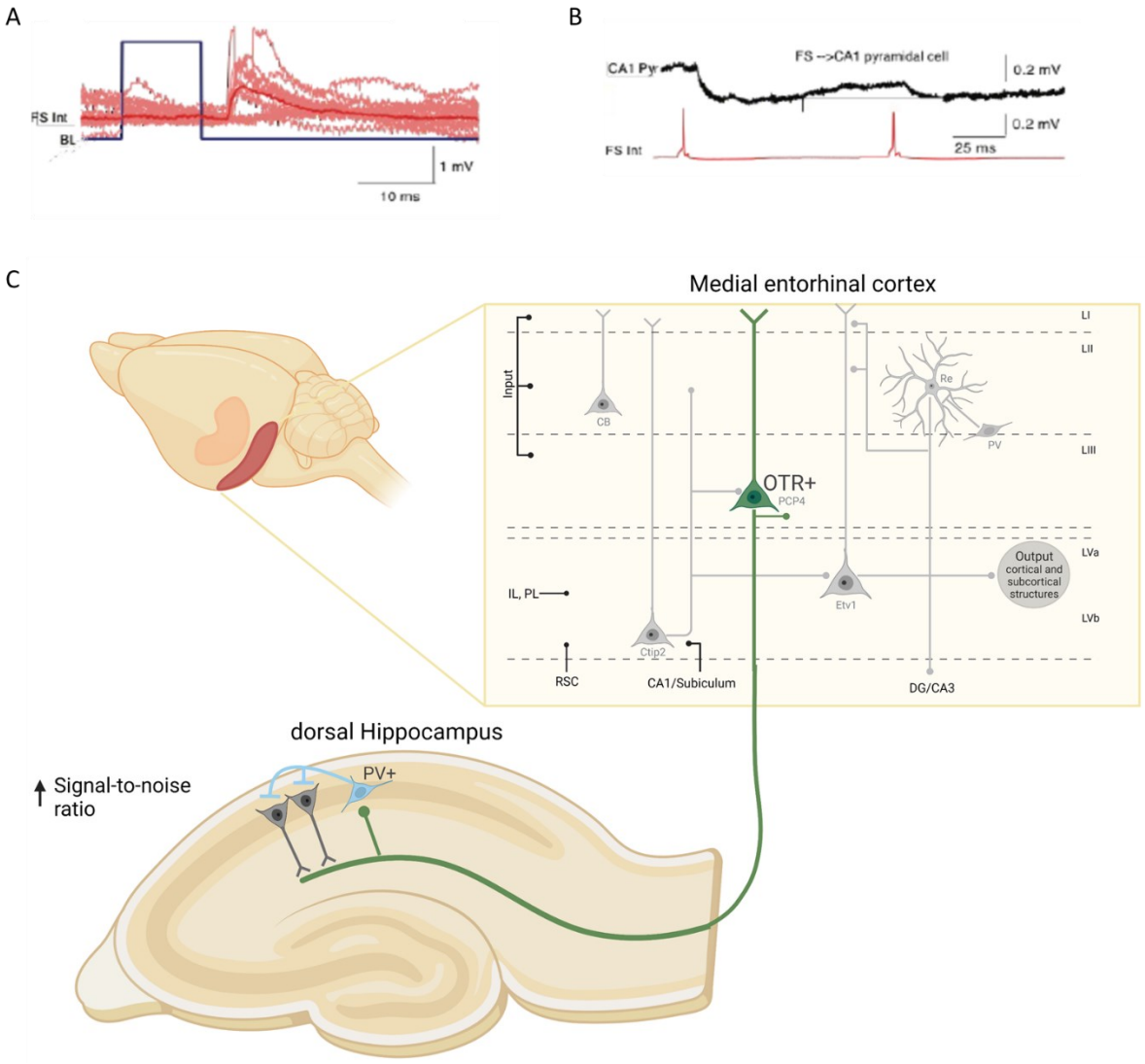

Figure 24: OTR+ MEC layer III neurons innervate interneurons in dorsal CA1. (A) Cre-dependent ChR2 AAV was injected in MEC. Following expression, ex vivo *electrophysiology was performed on horizontal slices via recording of potential post-synaptic neurons. Shining blue light (BL), indicated by black line, on axon terminals led to EPSPs in fast-spiking (FS) interneurons. Traces are shown in red. (B) Pair recording of a CA1 FS interneuron and a CA1 pyramidal neuron. Activation of the interneuron (in red) upon BL illumination resulted in IPSP generation in the pyramid neuron (in black). These preliminary results were provided by Dr. Julia Lebedeva. (C) OT-sensitive MEC to CA1 pathway. OTR+ neuron (green) of MEC layer III innervates an interneuron in CA1. This interneuron connects to several CA1 pyramid neurons resulting in a feed-forward inhibition pathway. Created with BioRender.com*

In complement to presented anterograde tracing experiment, a preliminary *ex vivo* electrophysiology recording was performed to investigate the innervation of the dorsal CA1 cells by OTR+ MEC neurons. For this experiment Cre-dependent Channelrhodopsin 2 (ChR2) expressing AAV was injected into the MEC of OTR-IRES-Cre knock-in rats. Following virus expression, *ex vivo* electrophysiology was performed on horizontal hippocampal slices. CA1 region was illuminated by blue light to activate ChR2 gated channels in the axon terminals from OTR+ MEC neurons. Upon activation of MEC OTR+ neuron axon terminals, increased

activity of interneurons was recorded (Figure 24A). Additional pair recordings revealed that an interneuron activated by blue light evoked inhibitory postsynaptic currents (IPSCs) in a connected pyramid neuron (Figure 24B). Although results of this preliminary electrophysiological experiment are in line with anterograde viral tracing, it is known that MEC innervation of dorsal CA1 also activates deep pyramidal neurons located towards CA2 region [37] and also some pyramidal neurons were found in anterograde tracing experiments. Thus, further electrophysiological investigation might reveal more complex connections especially in respect to OTR+ MEC axon populations. Nevertheless, based on these results, a potential model of the signaling from OTR-expressing MEC neurons to hippocampus neurons can be proposed. As shown in Figure 24C, axons from OTR+ layer III PCs of the MEC preferentially terminate onto interneurons of the dorsal CA1, which in turn, form inhibitory synapses on CA1 PCs. This network would be well in line with previously described innervation of CA1 by MEC layer III as feed-forward inhibition of PCs in hippocampus is one of the main generally accepted signaling pathways [35]. Additionally, the activation of OTR signaling in hippocampal interneurons has also been described to increase their inhibitory input on PCs [74,78], thus, acting in a similar way and supporting the idea that OT might act on paralleling pathways to improve the signal-to-noise ratio and sharpen responses of PCs to salient stimuli, including social subjects [47].

4.3 Do OTR+ MEC cells modulate social and spatial behaviors?

4.3.1 Experimental paradigms

In the course of my PhD work, I used two well-established behavior paradigms, applied in OT field and in hippocampal studies [61,80,91,109,110]. Social memory has been reported to be reliant on processing in the dCA2/CA3 region of hippocampus and impaired in region specific OTR knock-out mice [73,83]. Thus, I decided to first investigate the effect of silencing or ablation of OTR+ MEC neurons on social memory. Furthermore, spatial navigation to social partners is relevant for initiation of social behaviors. It has been recently reported that place cells in dorsal CA1 region show firing fields for the location of a conspecific animal [91]. As place cells in CA1 receive input from MEC layer III neurons, I proposed that OTR+ MEC neurons can be involved in shaping socially-relevant place fields in analogy to firing fields of MEC neurons and grid fields during movements towards food reward locations [89,90]. Thus, secondly, I designed a behavioral setting using T-Maze to investigate the involvement of OTR+ MEC neurons in the learning of and navigation to social vs. food reward locations.

4.3.2 OTR+ MEC neurons and social memory

4.3.2.1 Experimental setting and interpretation of results

Chemogenetic silencing or ablation of OTR+ MEC cells did not affect social interaction time between conspecifics.

To test the effect on social memory retrieval, OTR+ MEC neurons were silenced during the social memory test, but not during the learning period. In this case, there was no significant difference, but a trend towards reduced social memory was found.

Both in the chemogenetic silencing and the ablation experiment, intraindividual differences were quite high, in line with a recent study [109] using a similar setup. As this was not the case during free social interaction, it might be due to a loss of social interest in the interaction with caged conspecifics that is different between individual animals.

In addition, the preference in the control group for the novel conspecific was only at about 60%. For a loss of social memory, it would be expected that the test rats show no preference, meaning they spent 50% of time with the novel rat and the familiar rat, respectively [80]. The relatively low preference for the novel rat in the control group reduced the potential difference between both groups to about 10%. This issue will be discussed in detail below.

Since I found that the control group showed only low preference for the unfamiliar conspecific during the social memory test, I modified the paradigm to improve social memory in the control group for the second experiment with eliminated OTR+ MEC neurons by extension of the acquisition period to 20 min and reduction of the period between memory acquisition and memory test to 1 h. However, even with the adjusted paradigm, the control group only showed a small preference for interacting with the novel conspecific when the data was viewed as time spent with the novel conspecific as proportion of the cumulative interaction time.

Deeper analysis of the video files using the TrackRodent system published by Nester et al, 2019 [95] revealed that both in Caspase and control group the time spent investigating the novel stimulus was higher than the familiar conspecific during the social memory test through this preference for the unfamiliar conspecific was not significant. Additionally, the long bouts (more than 7 sec) of investigation were also increased for the novel stimulus animal, although this difference remains not significant either. One of the reasons for this were the high variabilities between animals. Though not significant these trends fit to what is published for social memory in rats, where a higher number (up to 60) of animals was used [109].

In general, the OTR-IRES-Cre rat model might not be the easiest system to test changes in social memory. Netser et al, 2020 had previously reported that Sprague Dawley rats show less

preference for a novel stimulus in a memory test compared to C57BL/6J mice or Wistar Hannover rats. In a similar social memory test, they could however show that long bouts of investigation are significantly increased for the novel stimulus [109].

4.3.2.2 How to improve settings and tools in prospective experiments?

To improve readout of these initial experiments, first of all a higher number of animals should be included in order to decrease variance and improve the distinction between the novel and familiar conspecific over the group. It would also be a possibility to do the social memory test with two freely moving conspecifics to increase the cumulative interaction time [61]. Also, cage mate animals can be primarily tested as they spent more time freely interacting with each other and should show consistent preference for a novel conspecific in a social memory test [80]. Though there were no differences seen in the deletion experiment, the trend for an impaired social memory when OTR+ cells were inhibited during the social memory test in the chemogenetic trial suggests that further experiments might be useful. As Sprague Dawley rats do not show a strong preference for the novel stimulus in the social memory test [109], it might be valuable to use Gq manipulation (opposingly to used silencing DREADD subunit) to activate OTR+ MEC neurons during the social memory test and try to enhance social memory.

4.3.3 OTR+ MEC cells and learning of a social vs. food reward location

4.3.3.1 Experimental settings and interpretation of results

In the chemogenetic experiments, no significant difference was found when OTR+ MEC neurons were silenced during the T-Maze test with a social reward. However, in this experiment the learning phase of the social reward location was not included in the chemogenetic manipulation. As it has been shown that the learning of spatial locations is impaired in MEC lesion experiments [88] and a deficit in working memory impaired learning of a reward location in a transgenic mouse model with a specific inhibition of the MEC layer III→hippocampus pathway [111], I decided to investigate the impact of silencing OTR+ MEC neurons in the memory acquisition phase of the T-Maze paradigm. To not subject the animals to daily injections of CNO during the learning period, the Caspase 3 AAV system was used to specifically delete OTR+ MEC neurons.

In animals with ablated OTR+ MEC neurons, learning of a social reward location was impaired. Curves calculated to fit the data points were significantly different between the two groups, even though, comparison of single data points yielded no significant results. The lack of significance for the latter is probably due to relatively high variances caused by the experimental setup with 5 trial runs per day and could be solved by increasing the number of

animals. Besides, the deletion group never reached a level of choosing the reward arm in 70% of trials, which was previously defined as a threshold for successful learning.

The most interesting and potentially most important result was obtained after comparison of the effect of OTR+ MEC neuron deletion on social vs. food reward learning. In the learning of the food reward location, there was no significant difference between the deletion and the control group. Both groups successfully learned the food reward location. When comparing the last day of the social vs. the food reward learning, a clear trend towards impaired learning of the social reward but not the food reward is observed in the deletion group even though this trend is not significant. In conclusion, this is a very promising finding showing that deletion of OTR+ MEC neurons impaired the learning of a social reward location but not a food reward location.

4.3.3.2 How to improve settings and tools in prospective experiments?

First of all, to improve results obtained so far, the experiment should be repeated to increase the number of animals and thus reduce individual variances. Next, the deletion of all OTR+ neurons in MEC might influence intrinsic networks as well as output pathways in addition to the one connecting to dorsal hippocampus CA1 region. Although, it was a suitable tool to tackle behaviors affected by OTR+ MEC cells, for further investigation on the OT-sensitive MEC to hippocampus pathway a more specific approach is required. To specifically manipulate the OT-sensitive MEC layer III → CA1 pathway, a chemogenetic or optogenetic approach could be implemented. Due to the possibility to manipulate the activity of the circuit longer, a chemogenetic approach may be seen as preferable. In this case, Cre-dependent Gi or Gq can be expressed in OTR+ neurons of MEC, followed by local infusion of CNO in the dorsal CA1 via an implanted cannula. Using this approach, we may achieve specific activation or inhibition of only those CA1 neurons which receive synaptic input exclusively from OTR+ MEC cells. To cover memory acquisition phase, infusion of CNO would need to be performed before each session of reward learning in T-Maze. The described experiment will be essential to functionally validate my results obtained after OTR+ cell deletion in the MEC and thus verify the involvement of OTR+ MEC neurons in social reward learning.

4.4 Functional architecture of OT-sensitive MEC → dorsal hippocampus pathway

4.4.1 OTR+ cell signaling in the MEC

Although very little is known about the intrinsic role of OTR+ neurons in ensembles of the MEC, my results allow me to make a few speculations concerning this question. I found that 92% of OTR-expressing neurons are layer III pyramid neurons putatively projecting to CA1 region of hippocampus. The other 8% consist of mainly interneurons distributed in layer II, III and V and some of them express parvalbumin. It was reported that PV interneurons of layer II/III inhibit Stellate cells [14], which innervate the DG and CA3 regions projecting to CA1. Therefore, it is possible that OTR+ interneurons of superficial MEC layers may adjust signaling in hippocampus CA1 region by reducing the input it receives through the MEC stellate neuron → CA3 → CA1 pathway. On the other hand, as Stellate cells have been mainly discussed as a candidate for grid cells [112,113], it seems unlikely that layer III PCs exhibit grid cell spatial firing pattern. It might be fitting however, that the PCs represent object-vector cell-like firing instead. Object-vector cells have been reported to fire in a specific distance and orientation to an object [21]. As my study showed that OTR+ MEC neurons are involved in the learning of the location of a conspecific, these cells might provide the so far unknown input to recently reported "social" place cells [91]. A current study showed that a subset of CA1 place cells has specific firing fields for the location of a conspecific [91]. MEC layer III OTR+ neuron input to the dorsal hippocampus might adjust the inhibition/excitation balance to initiate this "social" place cell firing. If this is the case, OTR+ MEC layer III cells might show firing patterns similar to object vector cells. However, instead of firing in a specific distance and orientation to an object, they would fire in a specific distance and orientation to a conspecific rat making them social-vector cells. A similar cell type activated by OT action has recently been proposed by our group and colleagues [10]. To test this hypothesis, OTR+ MEC cells need to be recorded in an open arena with an object vs. a confined conspecific (please also see Conclusions and Open Questions section). Upon moving the conspecific to a different location, a social-vector cell should readjust its firing location in analogy to object vector cells reported by Hoydal et al., 2019 [21].

4.4.2 Relevance of the OT-sensitive MEC → dorsal hippocampus pathway in social territoriality

Individual's location is largely determined by social aspects, such as personal territory or a "home" where familial conspecifics are safely living and/or mating with partners. As recently

discussed by us and colleagues [10], space can be divided into socially meaningful territories with adjustable spatial borders. Knowing the role of OT in modulation of sociability, it was not surprising that this neuropeptide may support the representation of social territories in the spatial maps of the brain. In line with this idea, results of my PhD thesis suggest that the modulation of social territoriality is mediated via the OT-sensitive MEC→dorsal hippocampus pathway. Furthermore, the fact that deletion of OTR-expressing neurons in the MEC impaired the learning of a socially relevant location, it can be speculated that OT action in the MEC might be necessary for memory formation of social locations and social spatial maps, respectively.

4.5. CONCLUSIONS AND OPEN QUESTIONS

In conclusion, in my thesis I made the first attempt to reveal the role of OT in socio-spatial behaviors. Although obtained behavioral results require further experiments, my work already provides the first evidence for factual existence of the OT-sensitive system within the MEC-hippocampal domain of the rat brain. Thus, to confirm or rebut my overarching hypothesis on the role of OT in modulation of territorial behavior, the following questions should be addressed:

- Is there a sub-population of OT neurons specifically innervating MEC and how does it get activated? Does modulation of the activity of these OT neurons lead to similar behavioral results?

- Do OTR+ MEC neurons show firing patterns comparable to those of object-vector cells if recorded in an area with a confined conspecific? Does manipulation of OT/OTR+ MEC cell input have an impact on recordings of “social” place cell in dorsal CA1?

- Is the discovered OTR+ interneuron population in dorsal CA1 the main post-synaptic cell type to OTR+ MEC neurons? Do OTR+ interneurons in CA1 also receive direct OT input? Do they receive input from other OTR+ neurons in other brain regions uniting OT action to the building of social spatial maps in the hippocampus?

- What are the output regions of social place cells of the hippocampus?

- Is the OT-sensitive system in the MEC-hippocampal domain similarly organized in other species or are there distinct interspecies differences?

At the end, it should be noted that the exploration of abovementioned critical points is not only important for our understanding of basic mechanisms of OT-mediated socio-spatial behaviors, but also is highly relevant to understand human mental diseases characterized by alterations in social and interpersonal space regulation [87,114,115,116].

Acknowledgements

First, I would like to thank my supervisor Prof. Dr. Valery Grinevich for the possibility to do my PhD in his lab and for his guidance and support of my PhD project.

I would like to especially thank Dr. Marina Eliava for being my technical and scientific mentor, teaching me injections and lending me all of her anatomical skills to help me reconstruct the OTR+ MEC circuits. Thank you for answering all of my questions, discussing project ideas and supporting me.

I thank Jonas Schimmer for teaching me injections and animal handling, and for helping me with behavioral experiments when a second set of hands were needed.

Additionally, I greatly appreciate the help of Dr. Julia Lebedeva, who did the first electrophysiological recordings to verify MEC OTR+ cell types, and the current work of Dr. Alan Kania, who is currently analyzing electrophysiological properties of the medial entorhinal → hippocampal pathway.

I thank all lab members for the great working atmosphere, your help, input and support and for a lot of fun during our Friday's happy hours.

I would like to thank Prof. Dr. Rainer Spanagel for jumping in as my second examiner on short notice as well as Dr. Claudio Acuna Goycolea and Dr. Annarita Patrizi for being part of my examination committee.

I also thank my TAC members Prof. Dr. Stephan Frings and Dr. Haikun Liu for their support and suggestions through the 4 years of my PhD.

In the end, I would like to thank all my friends and my family for supporting and helping me through the successful and especially difficult periods of this intriguing PhD journey.

References

[1] Poulter S, Hartley T, Lever C (2018) The Neurobiology of Mammalian Navigation. Current Biology Review 28, R1023–R1042. [1] Igarashi KM (2016) The entorhinal map of space. Brain Research 1637:177-187. doi: 10.1016/j.cub.2018.05.050.

[2] Rowland DC, Roudi Y, Moser M-B, Moser EI (2016) Ten years of grid cells. Annu. Rev. Neurosci 39:19–40. doi: 10.1146/annurev-neuro-070815-013824

[3] Hartley T, Lever C, Burgess N, O'Keefe J (2014) Space in the brain: how the hippocampal formation supports spatial cognition. Phil. Trans. R. Soc. B 369: 20120510. http://dx.doi.org/10.1098/rstb.2012.0510

[4] Jeffrey K (2018) Cognitive representations of spatial location. Brain and Neuroscience Advances Volume 2: 1 –5. https://doi.org/10.1177/2398212818810686

[5] Igarashi KM (2016) The entorhinal map of space. Brain Research 1637:177-187. http://dx.doi.org/10.1016/j.brainres.2015.10.041

[6] Börger L, Dalziel BD, Fryxell JM (2008) Are there general mechanisms of animal home range behaviour? A review and prospects for future research: Home range modelling. Ecology Letters, vol. 11, no 6, p. 637-650. doi: 10.1111/j.1461-0248.2008.01182.x

[7] Schafer M, Schiller D (2018) Navigating Social Space. Neuron 100(2): 476–489. doi:10.1016/j.neuron.2018.10.006.

[8] Froemke RC, Young LJ (2021) Oxytocin, Neural Plasticity, and Social Behavior. Annual Review Neuroscience 44:359-381. doi: 10.1146/annurev-neuro-102320-102847.

[9] Anacker AMJ, Beery AK (2013) Life in groups: the roles of oxytocin in mammalian sociality. Front Behav Neurosci. 2013 Dec 11;7:185. doi: 10.3389/fnbeh.2013.00185.

[10] Wirth S, Soumier A, Eliava M, Derdikman D, Wagner S, Grinevich V, Sirigu A (2021) Territorial blueprint in the hippocampal system. Trends in Cognitive Science S1364-6613(21)00152-2. doi: 10.1016/j.tics.2021.06.005.

[11] Moser M-B, Rowland DC, Moser EI (2015) Place cells, grid cells and memory. Cold Spring Harb Perspect Biol. 7(2):a021808. doi: 10.1101/cshperspect.a021808.

[12] Nilssen ES, Doan TP, Nigro MJ, Ohara S, Witter MP (2019) Neurons and networks in the entorhinal cortex: A reappraisal of the lateral and medial entorhinal subdivisions mediating parallel cortical pathways. Hippocampus. Volume29, Issue12, Pages 1238-1254. https://doi.org/10.1002/hipo.23145

[13] Canto CB, Wouterlood FG, Witter MP (2008) What Does the Anatomical Organization of the Entorhinal Cortex Tell Us? Neural Plasticity. Volume 2008, Article ID 381243, 18 pages, doi:10.1155/2008/381243

[14] Witter MP, Doan TP, Jacobsen B, Nilssen ES, Ohara S (2017) Architecture of the Entorhinal Cortex A Review of Entorhinal Anatomy in Rodents with Some Comparative Notes. Frontiers in Systems Neuroscience 11:46. doi: 10.3389/fnsys.2017.00046.

[15] Fuchs EC, Neitz A, Pinna R, Melzer S, Caputi A, Monyer H (2016) Local and Distant Input Controlling Excitation in Layer II of the Medial Entorhinal Cortex. Neuron. 89(1):194-208. doi: 10.1016/j.neuron.2015.11.029.

[16] Armstrong C, Wang J, Lee SY, Broderick J, Bezaire MJ, Lee S-H, Soltesz I (2016) Target-selectivity of parvalbumin-positive interneurons in layer II of medial entorhinal cortex in normal and epileptic animals. Hippocampus. 26(6):779-93. doi: 10.1002/hipo.22559.

[17] Tang Q, Ebbesen CL, Sanguinetti-Scheck JI, Preston-Ferrer P, Gundlfinger A, Winterer J, Beed P, Ray S, Naumann R, Schmitz D, Brecht M, Burgalossi A (2015) Anatomical Organization and Spatiotemporal Firing Patterns of Layer 3 Neurons in the Rat Medial Entorhinal Cortex. J Neurosci. 35(36):12346-54. doi: 10.1523/JNEUROSCI.0696-15.2015.

[18] Ray S, Burgalossi A, Brecht M, Naumann RK (2017) Complementary Modular Microcircuits of the Rat Medial Entorhinal Cortex. Front Syst Neurosci. 11:20. doi: 10.3389/fnsys.2017.00020

[19] Sürmeli G, Cosmin Marcu D, McClure C, Garden DLF, Pastoll H, Nolan MF (2015) Molecularly Defined Circuitry Reveals Input-Output Segregation in Deep Layers of the Medial Entorhinal Cortex. Neuron. 88(5):1040-1053. doi: 10.1016/j.neuron.2015.10.041.

[20] Ohara S, Onodera M, Simonsen OW, Yoshino R, Hioki H, Iijima T, Tsutsui K-I, Witter MP (2018) Intrinsic Projections of Layer Vb Neurons to Layers Va, III, and II in the Lateral and Medial Entorhinal Cortex of the Rat. Cell Reports 24, 107–116. doi: 10.1016/j.celrep.2018.06.014.

[21] Hoydal OA, Skytoen ER, Andersson SO, Moser M-B, Mover EI (2019) Object-vector coding in the medial entorhinal cortex. Nature. 400-404. doi: 10.1038/s41586-019-1077-7.

[22] Taube JS (2007) The head direction signal: origins and sensory-motor integration. Annu Rev Neurosci. 30:181-207. doi: 10.1146/annurev.neuro.29.051605.112854.

[23] Solstad T, Boccara CN, Kropff E, Moser M-B, Moser EI (2008) Representation of geometric borders in the entorhinal cortex. Science. 322(5909):1865-8. doi: 10.1126/science.1166466.

[24] Kropff E, Carmichael JE, Moser M-B, Moser EI (2015) Speed cells in the medial entorhinal cortex. Nature. 523(7561):419-24. doi: 10.1038/nature14622.

[25] Ye J, Witter MP, Moser M-B, Moser EI (2018) Entorhinal fast-spiking speed cells project to the hippocampus. Proc Natl Acad Sci U S A. 115(7):E1627-E1636. doi:10.1073/pnas.1720855115.

[26] Hafting T, Fyhn M, Molden S, Moser M-B, Moser EI (2005) Microstructure of a spatial map in the entorhinal cortex. Nature. 436(7052):801-6. doi: 10.1038/nature03721.

[27] Sargolini F, Fyhn M, Hafting T, McNaughton BL, Witter MP, Moser M-B, Moser EI (2006) Conjunctive representation of position, direction, and velocity in entorhinal cortex. Science. 312(5774):758-62. doi: 10.1126/science.1125572.

[28] Brun VH, Solstad T, Brun Kjelstrup K, Fyhn M, Witter MP, Moser M-B, Moser EI (2008) Progressive increase in grid scale from dorsal to ventral medial entorhinal cortex. Hippocampus. 18(12):1200-12. doi: 10.1002/hipo.20504.

[29] Stensola H, Stensola T, Solstad T, Froland K, Moser M-B, Moser EI (2012) The entorhinal grid map is discretized. Nature. 492(7427):72-8. doi: 10.1038/nature11649.

[30] Witter MP, Kleven H, Flatmoen AK (2017) Comparative Contemplations on the Hippocampus. Brain Behavior Evolution 90:15–24. doi: 10.1159/000475703.

[31] Fanselow MS, Dong H-W (2010) Are the Dorsal and Ventral Hippocampus Functionally Distinct Structures? Neuron 65(1):7-19. doi: 10.1016/j.neuron.2009.11.031.

[32] Schultz C, Engelhardt M (2014) Anatomy of the hippocampal formation. Front Neurol Neurosci. 34:6-17. doi: 10.1159/000360925.

[33] Lee S-H, Marchionni I, Bezaire M, Varga C, Danielson N, Lovett-Barron M, Losonczy A, Soltesz I (2014) Parvalbumin-Positive Basket Cells Differentiate among Hippocampal Pyramidal Cells. Neuron. 82(5):1129-44. doi: 10.1016/j.neuron.2014.03.034.

[34] Valero M, Menendez de la Prida L (2018) The hippocampus in depth: a sublayer-specific perspective of entorhinal-hippocampal function. Curr Opin Neurobiol. 52:107-114. doi: 10.1016/j.conb.2018.04.013.

[35] Bell KA, Delong R, Goswamee P, McQuiston AR (2021) The Entorhinal Cortical Alvear Pathway Differentially Excites Pyramidal Cells and Interneuron Subtypes in Hippocampal CA1. Cerebral Cortex. 31(5):2382-2401. doi: 10.1093/cercor/bhaa359.

[36] Kullmann DM (2011) Interneuron networks in the hippocampus. Curr Opin Neurobiology. 21(5):709-16. doi: 10.1016/j.conb.2011.05.006.

[37] Masurkar AV, Srinivas KV, Brann DH, Warren R, Lowes DC, Siegelbaum SA (2017) Medial and Lateral Entorhinal Cortex Differentially Excite Deep versus Superficial CA1 Pyramidal Neurons. Cell Reports. 18(1):148-160. doi: 10.1016/j.celrep.2016.12.012.

[38] Chevaleyre V, Siegelbaum SA (2010) Strong CA2 Pyramidal Neuron Synapses Define a Powerful Disynaptic Cortico-Hippocampal Loop. Neuron. 66(4):560-72. doi: 10.1016/j.neuron.2010.04.013

[39] Smith AS , Williams Avram SK, Cymerblit-Sabba A, Song J, Young WS (2016) Targeted activation of the hippocampal CA2 area strongly enhances social memory. Mol Psychiatry. 21(8):1137-44. doi: 10.1038/mp.2015.189

[40] Cymerblit-Sabba A, Smith AS, Williams Avram SK, Stackmann M, Korgan AC, Tickerhoof MC, Young WS (2020) Inducing Partner Preference in Mice by Chemogenetic Stimulation of CA2 Hippocampal Subfield. Front Mol Neurosci. 13:61. doi: 10.3389/fnmol.2020.00061.

[41] van Strien NM, Cappaert NLM, Witter MP (2009) The anatomy of memory: an interactive overview of the parahippocampal-hippocampal network. Nat Rev Neurosci. 10(4):272-82. doi: 10.1038/nrn2614.

[42] Grinevich V, Knobloch-Bollmann HS, Eliava M, Busnelli M, Chini B (2016) Assembling the Puzzle: Pathways of Oxytocin Signaling in the Brain. Biol Psychiatry. 79(3):155-64. doi: 10.1016/j.biopsych.2015.04.013.

[43] Althammer F, Jirikowski G, Grinevich V (2018) The oxytocin system of mice and men-Similarities and discrepancies of oxytocinergic modulation in rodents and primates. Peptides. 109:1-8. doi: 10.1016/j.peptides.2018.09.003.

[44] Knobloch HS, Grinevich V (2014) Evolution of oxytocin pathways in the brain of vertebrates. Front Behav Neurosci. 8:31. doi: 10.3389/fnbeh.2014.00031.

[45] Knobloch S, Charlet A, Hoffmann LC, Eliava M, Khrulev S, Cetin AH, Osten P, Schwarz MK, Seeburg PH, Stoop R, Grinevich V (2012) Evoked axonal oxytocin release in the central amygdala attenuates fear response. Neuron. 73(3):553-66. doi: 10.1016/j.neuron.2011.11.030.

[46] Althammer F, Grinevich V (2017) Diversity of oxytocin neurons: beyond magno- and parvocellular cell types? J Neuroendocrinol. doi: 10.1111/jne.12549.

[47] Grinevich V, Stoop R (2018) Interplay between Oxytocin and Sensory Systems in the Orchestration of Socio-Emotional Behaviors. Neuron. 99(5):887-904. doi: 10.1016/j.neuron.2018.07.016.

[48] Zhang B, Qui L, Xiao W, Ni H, Chen L, Wang F, Mai W, Wu J, Bao A, Hu H, Gong H, Duan S, Li A, Gao Z (2021) Reconstruction of the Hypothalamo-Neurohypophysial System and Functional Dissection of Magnocellular Oxytocin Neurons in the Brain. Neuron. 109(2):331-346.e7. doi: 10.1016/j.neuron.2020.10.032.

[49] Eliava M, Melchior M, Knobloch-Bollmann H-S., Wahis J, da Silva Gouveia M, Tang Y, Ciobanu AC, Triana del Rio R, Roth LC, Althammer F, Chavant V, Goumon Y, Gruber T, Petit-Demouliere N, Busnelli M, Chini B, Tan LL, Mitre M, Froemke RC, Chao MV, Giese G, Sprengel R, Kuner R, Poisbeau P, Seeburg PH, Stoop R, Charlet A, Grinevich V (2016). A New Population of Parvocellular Oxytocin Neurons Controlling Magnocellular Neuron Activity and Inflammatory Pain Processing. Neuron. 89(6):1291-1304. doi: 10.1016/j.neuron.2016.01.041.

[50] Grinevich V, Ludwig M (2021) The multiple faces of the oxytocin and vasopressin systems in the brain. J Neuroendocrinol. e13004. doi: 10.1111/jne.13004.

[51] Ludwig M, Leng G (2006) Dendritic peptide release and peptide-dependent behaviours. Nat Rev Neurosci. 7(2):126-36. doi: 10.1038/nrn1845.

[52] Mitre M, Minder J, Morina EX, Chao MV, Froemke RC (2018) Oxytocin Modulation of Neural Circuits. Curr Top Behav Neurosci. 35:31-53. doi: 10.1007/7854_2017_7.

[53] Jurek B, Neumann ID (2018) The Oxytocin Receptor: From Intracellular Signaling to Behavior. Physiol Rev. 98(3):1805-1908. doi: 10.1152/physrev.00031.2017.

[54] Busnelli M, Chini B (2018) Molecular Basis of Oxytocin Receptor Signalling in the Brain: What We Know and What We Need to Know. Curr Topics Behav Neurosci. 35:3-29. doi: 10.1007/7854_2017_6.

[55] Chini B, Verhage M, Grinevich V (2017) The Action Radius of Oxytocin Release in the Mammalian CNS: From Single Vesicles to Behavior. Trends Pharmacol Sci. 38(11):982-991. doi: 10.1016/j.tips.2017.08.005.

[56] Hasan M, Althammer F, Silva da Gouveia M, Goyon S, Eliava M, Lefevre A. Kerspern D, Schimmer J, Raftogianni A, Wahis J, Knobloch-Bollmann S, Tang Y, Liu X, Jain A, Chavant V, Goumon Y, Weislogel J-M, Hurlemann R, Herpertz S, Pitzer C, Darbon P, Dogbevia GK, Bertocchi I, Larkum ME, Sprengel R, Bading H, Charlet A, Grinevich V (2019) A Fear Memory Engram and Its Plasticity in the Hypothalamic Oxytocin System. Neuron. 103(1):133-146. doi: 10.1016/j.neuron.2019.04.029.

[57] Grinevich V, Neumann ID (2021) Brain oxytocin: how puzzle stones from animal studies translate into psychiatry. Molecular Psychiatry 26:265-279. doi: 10.1038/s41380-020-0802-9.

[58] Carter CS , Kenkel WM , MacLean EL , Wilson SR , Perkeybile AM, Yee JR , Ferris CF, Nazarloo HP, Porges SW , Davis JM, Connelly JJ, Kingsbury MA (2020) Is Oxytocin "Nature's Medicine"? Pharmacol Review 72:829-861. doi: 10.1124/pr.120.019398.

[59] Lee H-J, Macbeth AH, Pagani JH, Young WS (2009) Oxytocin: the great facilitator of life. Prog Neurobiol. 88(2):127-51. doi: 10.1016/j.pneurobio.2009.04.001.

[60] Marlin BJ, Froemke RC (2017) Oxytocin modulation of neural circuits for social behavior. Dev Neurobiol. 77(2):169-189. doi: 10.1002/dneu.22452.

[61] Tang Y, Benusiglio D, Lefevre A, Hilfiger L, Althammer F, Bludau A, Hagiwara A, Baudon A, Darbon P, Schimmer J, Kirchner MK, Roy RK, Wang S, Eliava M, Wagner S, Oberhuber M, Conzelmann KK, Schwarz M, Stern JE, Leng G, Neumann ID, Charlet A, Grinevich V (2020) Social touch promotes interfemale communication viaactivation of parvocellular oxytocin neurons. Nature Neuroscience 23 (9), pp.1125-1137. doi: 10.1038/s41593-020-0674-y.

[62] Rilling JK, Young LJ (2014) The biology of mammalian parenting and its effect on offspring social development. Science. 345(6198):771-6. doi: 10.1126/science.1252723.

[63] Yoshihara C, Numan M, Kuroda KO (2018) Oxytocin and Parental Behaviors. Curr Top Behav Neurosci. 35:119-153. doi: 10.1007/7854_2017_11.

[64] Scott N, Prigge M, Yizhar O, Kimchi T (2015) A sexually dimorphic hypothalamic circuit controls maternal care and oxytocin secretion. Nature. 525(7570):519-22. doi: 10.1038/nature15378.

[65] Carcea I, Froemke RC (2019) Biological mechanisms for observational learning. Curr Opin Neurobiol. 54:178-185. doi: 10.1016/j.conb.2018.11.008.

[66] Ross HE, Young LJ (2009) Oxytocin and the Neural Mechanisms Regulating Social Cognition and Affiliative Behavior. Front Neuroendocrino 30(4): 534–547. doi: 10.1016/j.yfrne.2009.05.004.

[67] Keebaugh AC, Barrett CE, Laprairie JL, Jenkins JJ, Young LJ (2015) RNAi knockdown of oxytocin receptor in the nucleus accumbens inhibits social attachment and parental care in monogamous female prairie voles. Soc Neurosci. 10(5):561-70. doi: 10.1080/17470919.2015.1040893.

[68] Spengler FB, Scheele D, Marsh M, Kofferath C, Flach A, Schwarz S, Stoffel-Wagner B, Maier W, Hurlemann R (2017) Oxytocin facilitates reciprocity in social communication. Soc Cogn Affect Neurosci. 12(8):1325-1333. doi: 10.1093/scan/nsx061.

[69] Ferreti V, Maltese F, Contarini G, Nigro M, Bonavia A, Huang H, Gigliucci V, Morelli G, Scheggia D, Managò F, Castellani G, Lefevre A, Cancedda L, Chini B, Grinevich V, Papaleo F (2019) Oxytocin Signaling in the Central Amygdala Modulates Emotion Discrimination in Mice. Curr Biol. 29(12):1938-1953.e6. doi: 10.1016/j.cub.2019.04.070.

[70] Montagrin A, Saiote C, Schiller D (2018) The social hippocampus. Hippocampus. 28(9):672-679. doi: 10.1002/hipo.22797.

[71] Cilz NI, Cymerblit-Sabba A, Young WS (2019) Oxytocin and vasopressin in the rodent hippocampus. Genes, Brain and Behavior. 2019;18:e12535. doi: 10.1111/gbb.12535.

[72] Mitre M, Marlin BJ, Schiavo JK, Morina E, Norden SE, Hackett TA, Aoki CJ, Chao MV, Froemke RC (2016) A Distributed Network for Social Cognition Enriched for Oxytocin Receptors. J Neurosci. 36(8):2517-35. doi: 10.1523/JNEUROSCI.2409-15.2016.

[73] Raam T, McAvoy KM, Besnard A, Veenema AH, Sahay A (2017) Hippocampal oxytocin receptors are necessary for discrimination of social stimuli. Nature Communications 8: 2001. doi: 10.1038/s41467-017-02173-0.

[74] Maniezzi C, Talpo F, Spaiardi P, Toselli M, Biella G (2019) Oxytocin Increases Phasic and Tonic GABAergic Transmission in CA1 Region of Mouse Hippocampus. Front Cell Neurosci. 13:178. doi: 10.3389/fncel.2019.00178.

[75] LinY-T, Chen C-C, Huang C-C, Nishimori K, Hsu K-S (2017) Oxytocin stimulates hippocampal neurogenesis via oxytocin receptor expressed in CA3 pyramidal neurons. Nat Commun. 8(1):537. doi: 10.1038/s41467-017-00675-5.

[76] Lin Y-T, Hsieh T-Y, Tsai T-C, Chen C-C, Huang C-C, Hsu K-S (2018) Conditional Deletion of Hippocampal CA2/CA3a Oxytocin Receptors Impairs the Persistence of Long-Term Social Recognition Memory in Mice. J Neurosci. 38(5):1218-1231. doi: 10.1523/JNEUROSCI.1896-17.2017.

[77] Tirko NN, Eyring KW, Carcea I, Mitre M, Chao MV, Froemke RC, Tsien RW (2018) Oxytocin Transforms Firing Mode of CA2 Hippocampal Neurons. Neuron. 100(3):593-608.e3. doi: 10.1016/j.neuron.2018.09.008.

[78] Owen SF, Tuncdemir SN, Bader PL, Tirko NN, Fishell G, Tsien RW (2013) Oxytocin enhances hippocampal spike transmission by modulating fast-spiking interneurons. Nature. 500(7463):458-62. doi: 10.1038/nature12330.

[79] Vaccari C, Lolait SJ, Ostrowski NL (1998) Comparative Distribution of Vasopressin V1b and Oxytocin Receptor Messenger Ribonucleic Acids in Brain. Endocrinology. 139(12):5015-33. doi: 10.1210/endo.139.12.6382.

[80] Hitti FL, Siegelbaum SA (2014) The hippocampal CA2 region is essential for social memory. Nature. 508(7494):88-92. doi: 10.1038/nature13028.

[81] Stevenson EL, Caldwell HK (2014) Lesions to the CA2 region of the hippocampus impair social memory in mice. Eur J Neurosci. 40(9):3294-301. doi: 10.1111/ejn.12689.

[82] Meira T, Leroy F, Buss EW, Oliva A, Park J, Siegelbaum SA (2018) A hippocampal circuit linking dorsal CA2 to ventral CA1 critical for social memory dynamics. Nat Commun. 9(1):4163. doi: 10.1038/s41467-018-06501-w.

[83] Okuyama T (2018) Social memory engram in the hippocampus. Neuroscience Research 129, 17–23. doi: 10.1016/j.neures.2017.05.007.

[84] Leung C, Cao F, Nguyen R, Joshi K, Aqrabawi AJ, Xia S, Cortez MA, Snead OC, Kim JC, Jia Z (2018) Activation of Entorhinal Cortical Projections to the Dentate Gyrus Underlies Social Memory Retrieval. Cell Reports 23, 2379–2391. doi: 10.1016/j.celrep.2018.04.073.

[85] Lee H-J, Caldwell HK, Macbeth AH, Tolu SG, Young WS (2008) A conditional knockout mouse line of the oxytocin receptor. Endocrinology. 149(7):3256-63. doi: 10.1210/en.2007-1710.

[86] Okuyama T, Kitamura T, Roy DS, Itohara S, Tonegawa S (2016) Ventral CA1 neurons store social memory. Science. 353(6307):1536-1541. doi: 10.1126/science.aaf7003.

[87] Leblanc H, Ramirez S (2020) Linking Social Cognition to Learning and Memory. J Neurosci. 40(46):8782-8798. doi: 10.1523/JNEUROSCI.1280-20.2020.

[88] Hales JB, Schlesiger MI, Leutgeb JK, Squire LR, Leutgeb S, Clark RE (2014) Medial Entorhinal Cortex Lesions Only Partially Disrupt Hippocampal Place Cells and Hippocampus-Dependent Place Memory. Cell Reports 9, 893–901. doi: 10.1016/j.celrep.2014.10.009.

[89] Butler WN, Hardcastle K, Giocomo LM (2019) Remembered reward locations restructure entorhinal spatial maps. Science 363, 1447–1452. doi: 10.1126/science.aav5297.

[90] Boccara CN, Nardin M, Stella F, O'Neill J, Csicsvari J (2019) The entorhinal cognitive map is attracted to goals. Science 363, 1443–1447. doi: 10.1126/science.aav4837.

[91] Danjo T, Toyoizumi T, Fujisawa S (2018) Spatial representations of self and other in the hippocampus. Science. 359(6372):213-218. doi: 10.1126/science.aao3898.

[92] Danjo T (2020) Allocentric Representations of Space in the Hippocampus. Neuroscience Research. 153:1-7. doi: 10.1016/j.neures.2019.06.002.

[93] Oliva A, Fernandez-Ruiz A, Leroy F, Siegelbaum SA (2020) Hippocampal CA2 sharp-wave ripples reactivate and promote social memory. Nature. 587(7833):264-269. doi: 10.1038/s41586-020-2758-y.

[94] Zingg B, Chou X-I, Zhang Z, Mesik L, Liang F, Tao HW, Zhang LI (2017) AAV-mediated Anterograde Transsynaptic Tagging: Mapping Input-Defined Functional Neural Pathways for Defense Behavior. Neuron. 93(1):33-47. doi: 10.1016/j.neuron.2016.11.045.

[95] Netser S, Haskal S, Magalnik H, Bizer A, Wagner S (2019) A System for Tracking the Dynamics of Social Preference Behavior in Small Rodents. Journal of Visualized Experiments. (153). doi: 10.3791/60336.

[96] Yang CF, Chiang MC, Gray DC, Prabhakaran M, Alvarado M, Juntti SA, Unger EK, Wells JA, Shah NM. (2013) Sexually dimorphic neurons in the ventromedial hypothalamus govern mating in both sexes and aggression in males. Cell. 153(4):896-909. doi: 10.1016/j.cell.2013.04.017.

[97] MacLaren DAA, Browne RW, Shaw JK, Krishnan Radhakrishnan S, Khare P, Espana RA, Clark SD (2016) Clozapine N-Oxide Administration Produces Behavioral Effects in Long-Evans Rats: Implications for Designing DREADD Experiments. eNeuro. 3(5):ENEURO.0219-16.2016. doi: 10.1523/ENEURO.0219-16.2016.

[98] Roth BL (2016) DREADDs for Neuroscientists. Neuron. 89(4):683-94. doi: 10.1016/j.neuron.2016.01.040.

[99] Marlin BJ, Mitre M, D'amour JA, Chao MV, Froemke RC (2015) Oxytocin enables maternal behaviour by balancing cortical inhibition. Nature. 520(7548):499-504. doi: 10.1038/nature14402.

[100] Nakajima M, Görlich A, Heintz N (2014) Oxytocin modulates female sociosexual behavior though a specific class of prefrontal cortical interneurons. Cell. 159(2):295-305. doi: 10.1016/j.cell.2014.09.020.

[101] Melzer S, Michael M, Caputi A, Eliava M, Fuchs EC, Whittington MA, Monyer H (2012) Long-range-projecting GABAergic neurons modulate inhibition in hippocampus and entorhinal cortex. Science. 335(6075):1506-10. doi: 10.1126/science.1217139.

[102] Robert V, Cassim S, Chevaleyre V, Piskorowski RA (2018) Hippocampal area CA2: properties and contribution to hippocampal function. Cell Tissue Res. 373(3):525-540. doi: 10.1007/s00441-017-2769-7.

[103] Cui Z, Gerfen CR, Young WS (2013) Hypothalamic and other connections with dorsal CA2 area of the mouse hippocampus. J Comp Neurol. 521(8):1844-66. doi: 10.1002/cne.23263.

[104] Kohara K, Pignatelli M, Rivest AJ, Jung H-Y, Kitamura T, Suh J, Frank D, Kajikawa K, Mise N, Obata Y, Wickerham IR, Tonegawa S (2014) Cell type-specific genetic and optogenetic tools reveal hippocampal CA2 circuits. Nat Neurosci. 17(2):269-79. doi: 10.1038/nn.3614.

[105] Dudek SM, Alexander GM, Farris S (2016) Rediscovering area CA2: unique properties and functions. Nat Rev Neurosci. 17(2):89-102.doi: 10.1038/nrn.2015.22.

[106] Müller C, Remy S (2017) Septo–hippocampal interaction. Cell and Tissue Research. 373(3):565-575. doi: 10.1007/s00441-017-2745-2.

[107] Gonzalez-Sulser A, Parthier D, Candela A, McClure C, Pastoll H, Garden D, Sürmeli G, Nolan MF (2014) GABAergic Projections from the Medial Septum Selectively Inhibit Interneurons in the Medial Entorhinal Cortex. The Journal of Neuroscience 34(50):16739 – 16743.

[108] Lefevre A, Benusiglio D, Tang Y, Krabichler Q, Charlet A, Grinevich V (2021) Oxytocinergic Feedback Circuitries: An Anatomical Basis for Neuromodulation of Social Behaviors. Front Neural Circuits. 15:688234. doi: 10.3389/fncir.2021.688234.

[109] Netser S, Meyer A, Magalnik H, Zylbertal A, Haskal de la Zerda S, Briller M, Bizer A, Grinevich V, Wagner S (2020) Distinct dynamics of social motivation drive differential social behavior in laboratory rat and mouse strains. Nature Communications. 11(1):5908. doi: 10.1038/s41467-020-19569-0.

[110] Wenk GL (2001) Assessment of spatial memory using the T maze. Curr Protoc Neurosci. Chapter 8:Unit 8.5B. doi: 10.1002/0471142301.ns0805bs04.

[111] Suh J, Rivest AJ, Nakashiba T, Tominaga T, Tonegawa S (2011) Entorhinal Cortex Layer III Input to the Hippocampus Is Crucial for Temporal Association Memory. Science. 334(6061):1415-20. doi: 10.1126/science.1210125.

[112] Rowland DC, Obenhaus HA, Skytoen ER, Zhang Q, Kentros CG, Moser EI, Moser M-B (2018) Functional properties of stellate cells in medial entorhinal cortex layer II. Elife. 7:e36664. doi: 10.7554/eLife.36664

[113] Gu Y, Lewallen S, Kinkhabwala AA, Domnisoru C, Yoon K, Gauthier JL, Fiete IR, Tank DW (2018) A Map-like Micro-Organization of Grid Cells in the Medial Entorhinal Cortex. Cell. 175(3):736-750.e30. doi: 10.1016/j.cell.2018.08.066.

[114] Candini M, di Pellegrino G, Frassinetti F (2020) The plasticity of the interpersonal space in autism spectrum disorder. Neuropsychologia. 147:107589. doi: 10.1016/j.neuropsychologia.2020.107589.

[115] Asada K, Tojo Y, Osanai H, Saito A, Hasegawa T, Kumagaya S (2016) Reduced Personal Space in Individuals with Autism Spectrum Disorder. PLoS One. 11(1):e0146306. doi: 10.1371/journal.pone.0146306.

[116] Rice LJ, Einfeld SL (2015) Cognitive and behavioural aspects of Prader-Willi syndrome. Curr Opin Psychiatry. 28(2):102-6. doi: 10.1097/YCO.0000000000000135.

List of Figures

List of Tables